Mechanistic Investigation of the Ce(III)-Chloride Photoredox Catalysis System: Understanding the Role of Alcohols as Additives

Qiaomu Yang,[†1,2] Ellen Song,[†1] Yu Wu,[1] Chenshuai Li,[1] Michael R. Gau,[1] Jessica M. Anna,[1,3] Eric J. Schelter,*[1] and Patrick J. Walsh*[1]

†denotes equal contribution

1. P. Roy and Diana T. Vagelos Laboratories, Department of Chemistry, University of Pennsylvania, 231 S. 34th St., Philadelphia, PA 19104 (USA)

2. Present address: Center for Nanoscale Materials, Argonne National Laboratory, Woodridge, Illinois 60517, United States.

3. Department of Chemistry, University of Pittsburgh, 219 Parkman Ave, Pittsburgh, Pennsylvania 15213, USA

KEYWORDS: cerium, alkoxide, photocatalysis, kinetics, mechanism.

ABSTRACT

Photocatalytic C–H activation is an emerging area of research. While cerium-chloride photocatalysts have been extensively studied, the role of alcohol additives in these systems remains a subject of ongoing discussion. It is demonstrated that photocatalyst $[NEt_4]_2[Ce^{IV}Cl_6]$ (**1**) produces •Cl and added alcohols exhibit zero-order kinetics. Prior studies by other researchers suggested that **1** and alcohols lead to cerium alkoxides [Ce–OR] and alkoxy radical intermediates. To understand these seemingly divergent mechanistic proposals, an expanded investigation comparing the cerium(IV) catalyst **1** and cerium(III) complex $[NEt_4]_3[Ce^{III}Cl_6]$ (**2**), which exhibits markedly different reactivity and C–H selectivity, is disclosed. Our findings reveal that alcohol additives accelerate the conversion of cerium(III) to cerium(IV) catalysts, forming key intermediates such as $[NEt_4]_2[Ce^{III}Cl_5(HOCH_3)]$ (**5**) and $[NEt_4]_2[Ce^{IV}Cl_5(OCH_3)]$ (**6**), driven by excited state di-*tert*-butyl azodicarboxylate (DBAD) under blue

light irradiation. The active complex **6** releases •OCH_3 radical, in sharp contrast to •Cl radicals initiated by cerium(IV) photoredox catalyst **1**. These different reactivity and selectivity profiles can be understood in the context of complex **5** generation, and *in situ* formation of base to afford complex **6**. Experimental validation shows enhanced selectivity toward C–H bonds with different reactivity with catalyst **1** and methanol upon the addition of base; and decreased selectivity with catalyst **2** and methanol upon the addition of acid. These findings unify the previously contrasting observations of cerium halide/alkoxide photocatalytic systems, and provide a comprehensive understanding on the essential role of base/acid an alcohol for selectivity and reactivity.

TOC graphic:

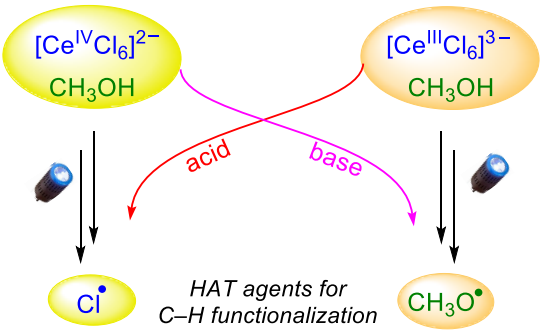

1. INTRODUCTION

Primary alkane C–H activation is an important endeavor for chemical research and industry.[1-9] Homogenous photocatalysts for alkane activation under mild conditions through ligand-to-metal charge transfer is an emerging field.[10] Recent advances include metal-oxyl,[11-13] and metal-halide photocatalysis.[14-35] And cerium photocatalysis has emerged as an important method in this domain. Cerium-chloride complexes exhibit desirable properties, such as visible light absorption, chlorine radical generation under light irradiation, mild ground state reduction potentials for catalysts turnover, and the potential for complementary photo-reduction through an independent, second-photon process.[30, 31, 33]

There has been an ongoing discussion on the influence of alcohols on the cerium photoredox catalysts.[28, 36-47] We have previously conducted an investigation into the $[Ce^{IV}Cl_6]^{2-}$ photoredox catalyst and demonstrated its ability to generate chlorine radicals that perform C–H activation, including with methane (**Scheme 1A**).[30] No influence of an $HOCH_2CCl_3$ additive under either stoichiometric or catalytic conditions was observed.[30] And it was found that light absorption by the cerium(IV) complex was the turnover-limiting step in the C–H functionalization reaction.[30] We also described the possibility of radical complexes of Cl· with alcohols or arenes,[48-54] and demonstrated how $HOCH_2CCl_3$ could show 'alkoxy radical-like' behavior in trapping experiments. And we described how radical-complexation could impact the selectivity in C–H activation experiments.[30, 48-54]

In a contrasting mechanistic hypothesis, Zuo and colleagues reported evidence for the generation of alkoxy radicals as active HAT agents in Ce-catalyzed reactions in the presence of alcohols (**Scheme 1B**). Specifically, they investigated the impact of $HOCH_2CCl_3$ on cerium(III/IV) catalysts in methane activation, proposing direct generation of an alkoxy radical intermediate from a Ce^{IV}–OR species.[29] They also identified alcohol-induced differences in selectivity in C–H activation of alkane substrates with inequivalent C–H bonds. Furthermore, with appropriate alcohol substrates they observed 1,5-hydrogen-atom abstraction (1,5-HAT) and beta-scission in cerium catalyzed reactions, which were proposed to proceed through alkoxy radicals.[28, 46, 55, 56] In a recent work, Zuo and co-workers further described C–H selectivity as a function of alcohol structure in the $Ce^{III}Cl_3$ system and provided computational electronic structure analysis of mixed cerium(IV) chloride alkoxide species.[28, 57] The conclusion by Zuo and co-workers is that cerium-alkoxides and alkoxy radicals rather than chlorine radicals are essential intermediates in C–H activation by cerium chlorides in the presence of alcohols.

These different mechanistic hypotheses of chlorine versus alkoxy radical intermediates, and our motivation to better understand cerium-based photoredox processes, inspired us to broaden our

investigation into the mechanism. There are two important differences between Zuo's and our catalyst systems: 1) the oxidation state of the catalytic cerium species (III and IV), and 2) the use of alcohols as additives. In past studies, the Zuo group has used both catalytic cerium(III/IV) while we have focused exclusively on cerium(IV) catalysts. An underlying assumption here was that the different oxidation states of the cerium species would yield similar results because Ce(IV) and Ce(III) are both intermediates in the proposed catalytic cycle. However, in the current work, we have observed notable differences in byproducts generated from an induction period when starting from $Ce^{III}Cl_3$ (with NEt_4Cl) or $[NEt_4]_3[Ce^{III}Cl_6]$. Crucially, the formation of the byproduct starting from $Ce^{III}Cl_3$ (with NEt_4Cl) or $[Ce^{III}Cl_6]^{3-}$ involves the formation of different intermediates that change the reaction mechanism and the structure of the active HAT agent (**Scheme 1C**). As evidenced in the current study, alcohols impact the induction reaction wherein the Ce(III) is oxidized to the radical-generating Ce(IV) intermediate, and impact the Ce(IV) photocatalyst speciation. In contrast, alcohols do not impact the catalytic cycle initiated with cerium(IV). We also demonstrate how the oxidation state of the catalytic cerium source, and the presence/absence of alcohols impact the reactivity and change the selectivity of the C–H functionalization reaction. Our results provide progress towards unifying the previous, outwardly disparate mechanistic proposals into an integrated mechanistic picture that is consistent with the results described by the Zuo group and our team. These results emphasize the critical role of the induction phase in forming the active catalyst and the significance of acid/base involvement in regulating the active radical species, offering valuable insights for new catalyst design.

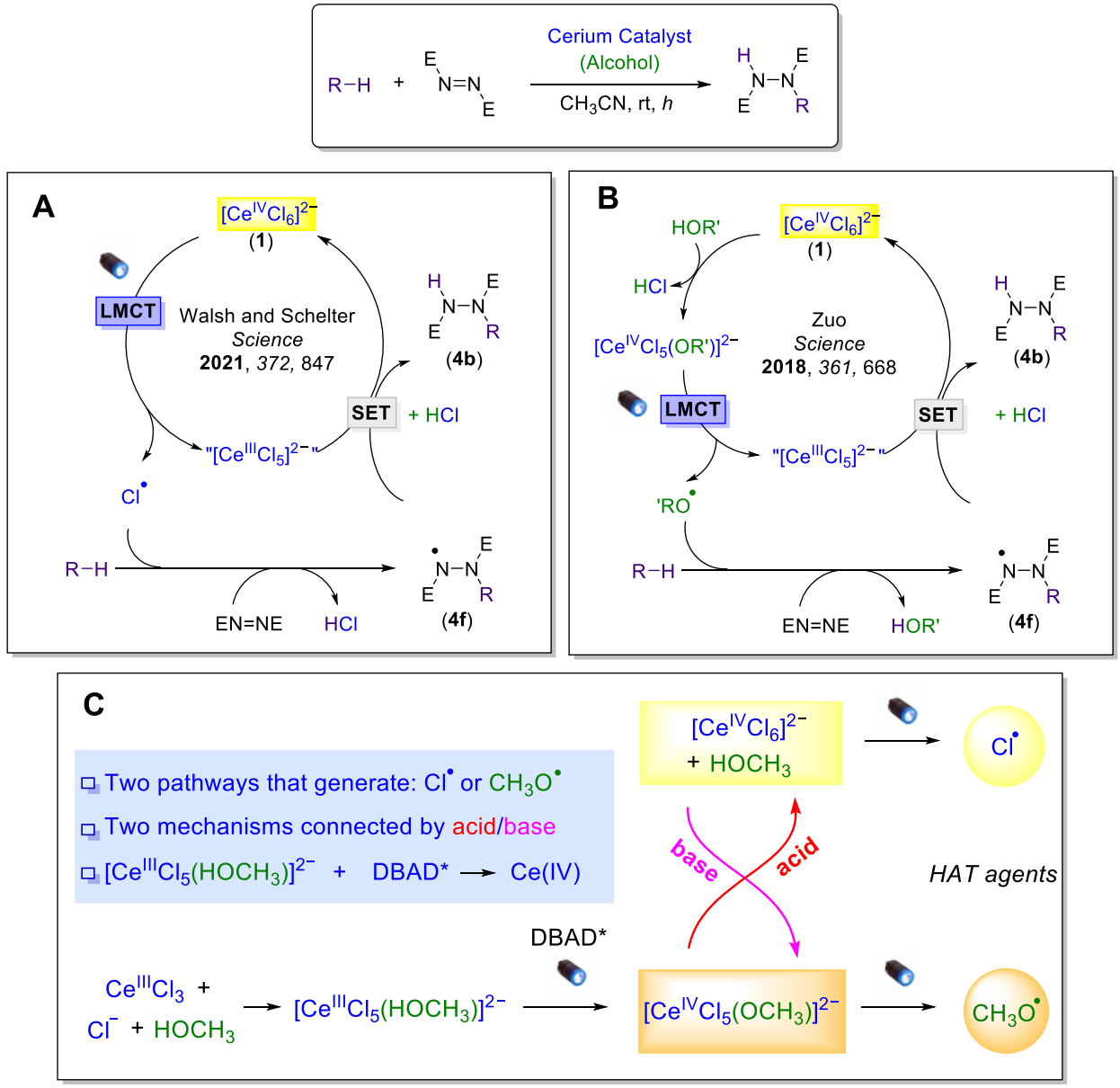

Scheme 1. A) Our proposed mechanism for alkane activation using the $[Ce^{IV}Cl_6]^{2-}$ photocatalyst. B) Proposed mechanism for alkane activation by Zuo *et al.* using the photoredox catalyst generated from $Ce^{III}Cl_3$, NEt_4Cl, and alcohol, or using $[(n\text{-}Bu_4N)_2][Ce^{IV}Cl_6]$ and alcohol. C) This work: proposed mechanism for alkane activation using Ce(IV) and Ce(III) photoredox catalysts and how these different catalytic cycles can be traversed by acid and base .

2. RESULTS AND DISCUSSION

2.1 On the Action of the $[Ce^{IV}Cl_6]^{2-}$ Photocatalyst and Generation of Chlorine Radical.

In previous work, we explored the C–H functionalization reactions of $[NEt_4]_2[Ce^{IV}Cl_6]$ (**1**) in various processes, including stoichiometric chlorinations,[30, 32] catalytic aminations,[31] and catalytic oxygenation reactions.[33] We proposed that chlorine radical was the reactive intermediate in all cases, and we demonstrated that the addition of alcohol such as $HOCH_2CCl_3$ did not affect the spectroscopic or reactivity properties of the $[Ce^{IV}Cl_6]^{2-}$ anion. As a result, cerium(IV) alkoxides (*e.g.*, $[Ce^{IV}Cl_5(OCH_2CCl_3)]^{2-}$) were excluded as active photoredox catalysts in our system starting from complex **1**.[30]

Furthermore in the current work, we probed the Ce(IV) species through static UV-vis absorption and probed the generation of chlorine radicals through transient absorption spectroscopic (TAS) studies of $[Ce^{IV}Cl_6]^{2-}$ in the presence of alcohols, in comparison with recent results from the Zuo group, where Ce–OR intermediates were described.[57] A UV-Vis spectrum of $[NEt_4]_2[Ce^{IV}Cl_6]$ (**1**, 1.64 mM) in CH_3CN was acquired. Addition of $HOCH_3$ (0.2 M) to the Ce(IV) solution was performed and another spectrum was collected. No substantial change in the absorbance maximum at 378 nm of $[NEt_4]_2[Ce^{IV}Cl_6]$ (**1**) was detected between these experiments (**Figure 1A**), whereas the alkoxide complex $[Ce^{IV}Cl_5(OCH_3)]^{2-}$ has a peak maximum at 344 nm.[28] These observations do not align with the previous proposal that $[Ce^{IV}Cl_6]^{2-}$ reacts with alcohols to generate cerium(IV) alkoxides, the proposed precursors to alkoxy radicals under visible light irradiation.[29] To understand the excited state chemistry of this system, transient absorption spectroscopic (TAS) experiments were performed. The TAS results showed that the addition of additives, including $HOCH_3$, $HOCH_2CCl_3$, benzene, and pyridinium chloride to $[Ce^{IV}Cl_6]^{2-}$ resulted in similar kinetic traces over the first 20 ps after photolysis (**Figure 1B**). A positive peak in the 320–350 nm range was observed and attributed to the transient chlorine radical

(Cl•) signal from bond homolysis of $[Ce^{IV}Cl_6]^{2-}$ in these experiments. In addition, an excited state absorption (ESA) peak in the 430–550 nm range was attributed to a cerium(III) species (see Supporting Information, Section II). Through a global target analysis, we found that most of the photo-generated Ce(III) species undergoes recombination with the chlorine radical to regenerate cerium(IV), while a small portion of the chlorine radical is observed as a non-decaying spectral feature on the 200 ps timescale (see Supporting Information, Section II). Analysis of possible chlorine radical-complexation on the nanosecond time scale was precluded due to the reported spectroscopic similarity among the chlorine radical complexes with acetonitrile, alcohols and halogenated solvents.[48, 49, 58]

Overall, our results demonstrated that the generation of chlorine radicals (Cl•) from $[Ce^{IV}Cl_6]^{2-}$ was not affected by the additives (alcohols or arenes) on the picosecond timescale. The observed photogeneration of Cl• from $[Ce^{IV}Cl_6]^{2-}$ is consistent with our previous mechanistic results using **1** as a photoredox catalyst.[30]

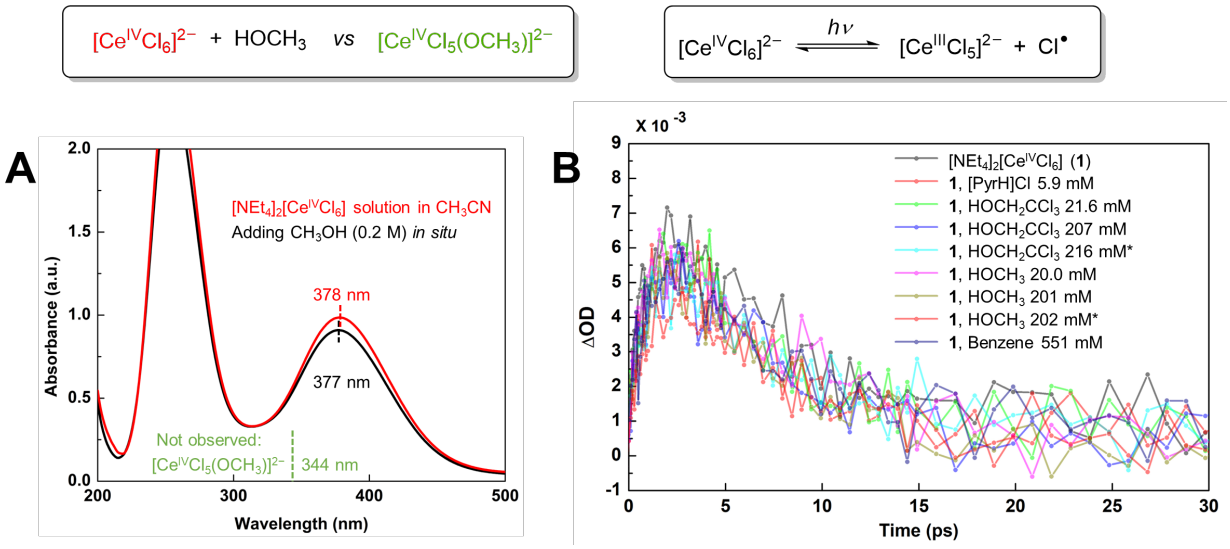

Figure 1. A) Static UV-Vis spectrum of $[NEt_4]_2[Ce^{IV}Cl_6]$ (**1**, 1.64 mM) solution in CH_3CN (red trace) and addition of $HOCH_3$ (0.2 M) *in situ* (black trace). The $[Ce^{IV}Cl_5(OCH_3)]^{2-}$ complex was not observed. B)

Transient absorption temporal traces of **1** at 334 nm with different additives at different concentrations. [PyrH]Cl = pyridinium chloride. The blue trace with asterisk*: 216 mM $HOCH_2CCl_3$ also contains 5.6 mM [PyrH]Cl. The red-orange trace with asterisk*: 202 mM $HOCH_3$ also contains 6.7 mM [PyrH]Cl.

2.2 Impact of Ce(III/IV) Complexes and Alcohol Additives on Reactivity

Although alcohol has a limited effect on the Ce(IV) catalyst, it evidently impacts the reaction when using Ce(III) complexes.[28] Having supported our hypothesis of chlorine radical intermediacy in the action of the $[NEt_4]_2[Ce^{IV}Cl_6]$ photoredox catalyst (**1**), we next turned our attention to the impact of cerium oxidation state (III/IV) and alcohol additives on the amination reaction **(Table 1**). Control experiments were conducted using either $[NEt_4]_2[Ce^{IV}Cl_6]$ (**1**) or $[NEt_4]_3[Ce^{III}Cl_6]$ (**2**), with or without $HOCH_2CCl_3$. The experimental conditions were based on a prior study conducted by our group and reported conditions by Zuo and co-workers.[29, 30] Here, we used 3 equiv cyclohexane and 1 equiv DBAD (**4a**) as the reaction substrates in acetonitrile under 467 nm blue light irradiation. The results showed that the use of catalytic $[NEt_4]_2[Ce^{IV}Cl_6]$ (**1**) led to a 47% yield of the C–H activation product (**4b**) at a low catalyst loading (0.5 mol%, **Table 1, Entry i**) and 84% yield at high catalyst loading (5 mol%, **Entry ii**) at 12 h. In previous studies, $HOCH_2CCl_3$ was found to have no effect on the $[NEt_4]_2[Ce^{IV}Cl_6]$ (**1**) photocatalyst and was, therefore, not included in the current study.[30]

Surprisingly, when using catalytic amounts of $[NEt_4]_3[Ce^{III}Cl_6]$ (**2**), only trace yields of C–H amination product **4b** were observed (**Entries iii–iv**). The addition of NEt_4Cl for these experiments was based on the previously-described equilibrium: 2 $[NEt_4]_3[Ce^{III}Cl_6]$ (**2**) ⇌ $[NEt_4]_3[Ce_2^{III}Cl_9]$ (**3**) + 3 $[NEt_4]Cl$,[31] to shift the catalyst speciation from the Ce(III) dimer **3** to Ce(III) monomer **2.** However,

even with the addition of NEt_4Cl, less than 2% conversion to **4b** was observed (**Entries vii, viii**), indicating that formation of the catalytically inactive dimer **3** is not the major cause of the low conversion of **4a** to **4b**. In previous reports, Zuo and co-workers proposed two different pathways for oxidation of Ce(III) to generate the Ce(IV) photocatalyst: 1) oxidation of $[Ce^{III}Cl_6]^{3-}$ with excited state DBAD*,[55] or 2) reduction of DBAD with an excited state cerium(III)-alcohol* species.[56] Under the current conditions (**Entries iii–iv**), where most of the 467 nm blue light was presumably absorbed by DBAD (**4a**), the absence of reactivity indicates the low reactivity for DBAD* to convert the $[Ce^{III}Cl_6]^{3-}$ to an active cerium(IV) photocatalyst.

However, the addition of $HOCH_2CCl_3$ accelerated catalysis, presumably by facilitating the formation of a cerium(IV) catalyst (**Entries v–vi, ix–x**), resulting in up to 29% yield of **4b**. The observation that alcohol impacts the initiation of the C–H activation prompted us to systematically explore the induction reactions.

Table 1. Cyclohexane amination reactions catalyzed by cerium photoredox catalysts **1** and **2**. The cerium oxidation states (III/IV) and presence of $HOCH_2CCl_3$ additive were examined. Catalyst loading and the presence of excess NEt_4Cl were also probed.

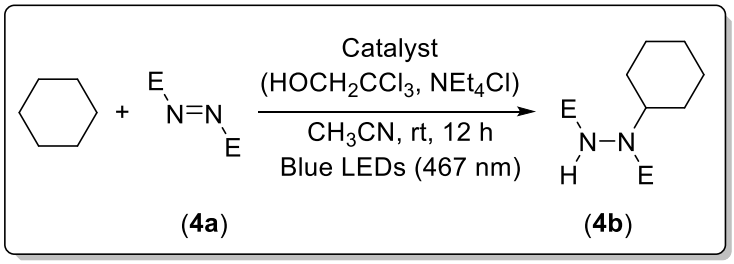

Entry	Catalyst	Cat. loading (per Ce)	NEt_4Cl	$HOCH_2CCl_3$	Yield
i	$[NEt_4]_2[Ce^{IV}Cl_6]$ (**1**)	0.5 mM	–	–	47 %
ii	**1**	5 mM	–	–	84 %
iii	$[NEt_4]_3[Ce^{III}Cl_6]$ (**2**)	0.5 mM	–	–	~ 0 %

iv	**2**	5 mM	–	–	~ 1 %
v	**2**	0.5 mM	–	20 mM	14 %
vi	**2**	5 mM	–	20 mM	16 %
vii	$[NEt_4]_3[Ce^{III}Cl_6]$ (**2**)	0.5 mM	1.0 mM	–	~ 0 %
viii	**2**	5 mM	10 mM	–	~ 1 %
ix	**2**	0.5 mM	1.0 mM	20 mM	6 %
x	**2**	5 mM	10 mM	20 mM	29 %

Given our observation that $HOCH_2CCl_3$ affects the amination reaction with catalytic Ce(III) complexes, we conducted a series of experiments to examine the cyclohexane amination reaction as a function of time (**Figure 2A**). In the experiments, we evaluated the impact of 1) cerium(III/IV) speciation, 2) different alcohol additives and 3) the impact of light sources on the reactivity, especially in the induction period. This data is shown graphically (**Figure 2B–D**) and discussed below.

To compare the effect of cerium(III/IV) speciation, $[NEt_4]_2[Ce^{IV}Cl_6]$ (**1**), $[NEt_4]_3[Ce^{III}Cl_6]$ (**2**), and $[NEt_4]_3[Ce_2^{III}Cl_9]$ (**3**) were used in the cyclohexane amination reaction (**Figure 2B, entries i, ii, iii**), with Tuna Blue light irradiation, without any alcohol additives. In the presence of 0.5 mM of $[NEt_4]_2[CeCl_6]$ (**1**), the C–H amination reaction proceeded the fastest and with the highest yield of amination product **4b** (**entry i**); a reaction yield of 19% after 2 h was measured, with 52% yield after 40 h. When the cerium(III) monomer $[NEt_4]_3[Ce^{III}Cl_6]$ (**2**) was used, the yield was 5% after 2 h, and 22% after 40 h (**entry ii**). The slower reaction can be attributed to the induction period, where $[NEt_4]_3[Ce^{III}Cl_6]$ was oxidized to a photoactive cerium(IV) species. In the case of the cerium(III) dimer $[NEt_4]_3[Ce^{III}_2Cl_9]$ (**3**), little product was observed, with a yield of 12% after 40 h (**entry iii**).

Next, we considered that the identity of the alcohol could play a significant role in the duration of the induction period with $[NEt_4]_3[Ce^{III}Cl_6]$ (**2**). Thus, ^{t}BuOH, $HOCH_2CCl_3$, and $HOCH_3$ were evaluated as additives (**Figure 2C**, **entries iv–vi**). We observed the shortest induction period and highest conversion when $HOCH_3$ was used, while ^{t}BuOH slowed the amination reaction. Both $HOCH_2CCl_3$ (**entry v**) and $HOCH_3$ (**entry iv**) resulted in higher conversions of **4a** to **4b**: 27% and 40% after 8 h, respectively, and 55% and 62% after 40 h; the same reaction performed in the absence of alcohol gave yields of 10% at 8 h and 22% at 40 h. Noteworthy, a byproduct, di-*tert*-butyl hydrazine carboxylate (**4c**) was observed over the course of the reaction (see Supporting Information, Section III), as previously noted.[29-30] We observed that $HOCH_3$ facilitates hydrazine **4c** generation compared with $HOCH_2CCl_3$ and ^{t}BuOH. The production of hydrazine **4c** occurred simultaneously with the formation of cyclohexane amination product **4b**, suggesting its production is continuous, and is further discussed in Section 2.4, *vide infra*.

In addition to alcohols, the light source employed for the catalytic C–H amination of cyclohexane was also observed to influence the reaction rates and yields. It has been described previously that both $[Ce^{III}Cl_6]^{3-}$ and DBAD absorb light and act as photoinitiators,[31, 59, 60] where $[Ce^{III}Cl_6]^{3-}$ absorbs UVA light and DBAD absorbs both blue and UVA light. The cerium(III) species **2** and **3** both absorb in the UVA region generating a super-reductant (–3.45 V vs Fc/Fc^+),[31] with their absorptions tailing into the purple region at 380 nm. Therefore, the 390 nm Kessil lamp, which extends to 370 nm, can excite **2** and **3** and may facilitate the conversion of cerium(III) to cerium(IV). However, using visible light sources, the optical density of the solution can largely be attributed to DBAD, due to its high absorbance (37 M^{-1} cm^{-1}) at 400 nm wavelength, suggesting that the DBAD* excited state might play a significant role in the induction reaction by oxidizing cerium(III) to cerium(IV). When the 476

nm Kessil lamp is used, we would expect DBAD* to initiate the induction process, as this light source produces little UV flux.

To compare the excited state species that impact the induction period as a function of light source, three different Kessil lamps (390 nm, 467 nm, and Tuna Blue) were used with $[NEt_4]_3[Ce^{III}Cl_6]$ (**2**) in the presence of $HOCH_3$ (0.2 M) for the amination of cyclohexane (**Figure 2D, entries iv, vii–viii**). The higher energy 390 nm irradiation resulted in the most product **4b** at 1 h (28% yield, **entry vii**), a result that indicates a faster induction reaction and the potential involvement of excited state cerium(III)* in the induction period under these conditions. Use of the broad-spectrum Tuna Blue (**entry iv**) or the 467 nm lamps (**entry viii**) both resulted in similar reactivity in the first 8 h, with approximately 4% yield after 1 h and 35–40% yield after 8 h. These results suggest that excited state DBAD* also behaves as a photoinitiator under blue light, though at a lower efficiency than Ce(III)* under Kessil 390 nm light irradiation. It should be noted that the three light sources have slightly different photon fluxes (See Supporting Information, Section III.VII, 390 nm light: Tuna blue: 467 nm light = 1.97: 1.38: 1.00 for light intensity).

The 467 nm light gave an overall lower yield (43% at 40 h) with $[Ce^{III}Cl_6]^{3-}$ than the Tuna Blue light (62% at 40 h, **Figure 2D**), likely due to the inefficient light absorption for DBAD and cerium(IV) species at the 467 nm wavelength. In the absence of $HOCH_3$ with 467 nm light, the reaction with $[Ce^{III}Cl_6]^{3-}$, only yields 9% C–H amination product **4b** after 16 h, and 15% after 40 h. Under identical conditions, but with $HOCH_3$ as an additive, 40% was measured at 16 h and 43% at 40 h (see Supporting Information Section III.VI). This result highlights the importance of $HOCH_3$, in combination with the excited state DBAD*, and will be further discussed in the next section.

Based on the above-mentioned analyses using different cerium sources, we conclude that cerium(III) was converted to cerium(IV) in the induction reaction, and that a cerium(IV) complex is the catalyst that generated the key intermediate in the HAT with cyclohexane. Alcohol additive experiments indicate that alcohols such as $HOCH_3$ and $HOCH_2CCl_3$ shorten the induction reaction. The light source experiments suggest that, under blue or 467 nm light irradiation, DBAD is likely to absorb the light and its excited state reacts with cerium(III) in the induction reaction; under 390 nm light irradiation, both DBAD and cerium(III) can absorb light.

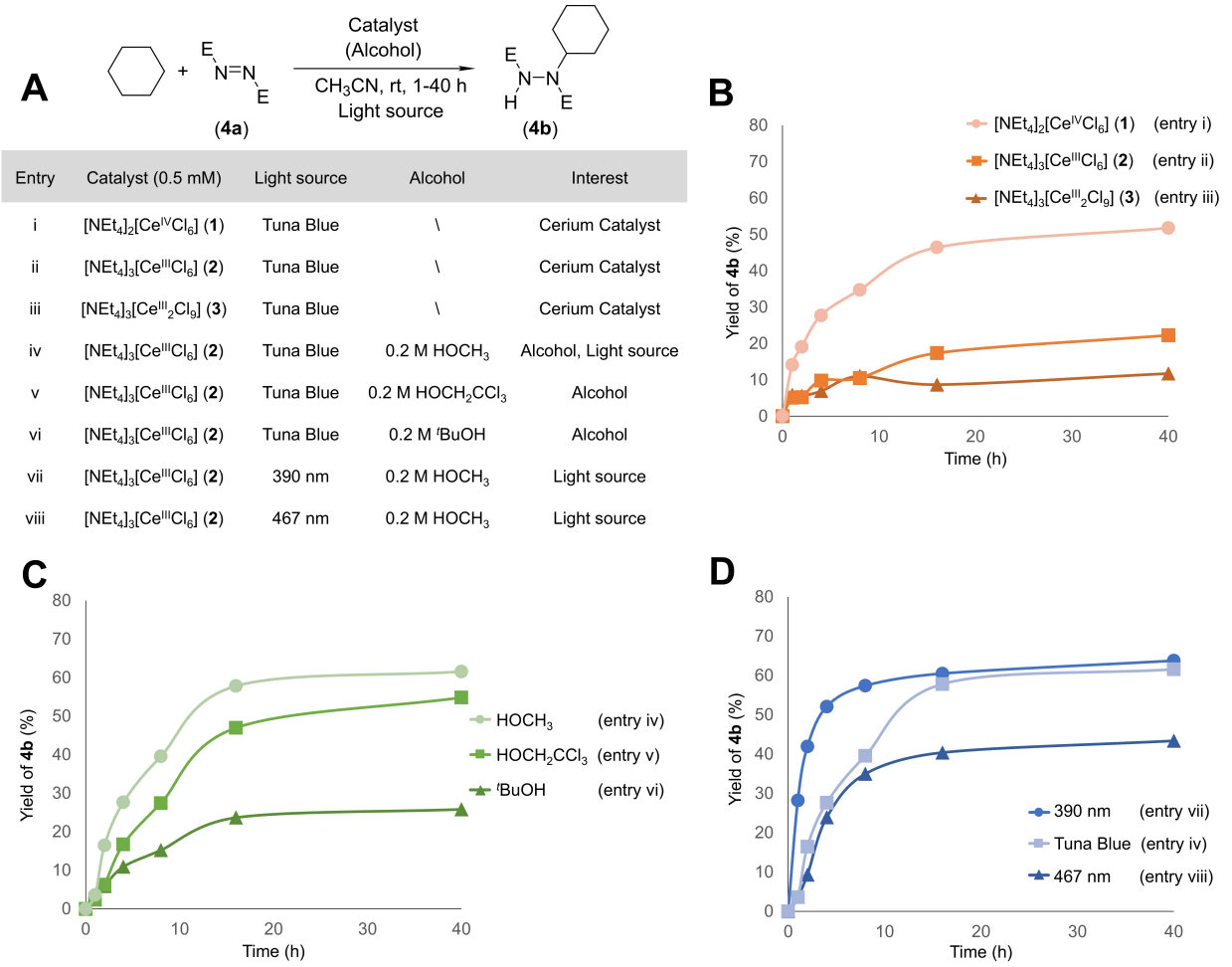

Entry	Catalyst (0.5 mM)	Light source	Alcohol	Interest
i	$[NEt_4]_2[Ce^{IV}Cl_6]$ (**1**)	Tuna Blue	\	Cerium Catalyst
ii	$[NEt_4]_3[Ce^{III}Cl_6]$ (**2**)	Tuna Blue	\	Cerium Catalyst
iii	$[NEt_4]_3[Ce^{III}_2Cl_9]$ (**3**)	Tuna Blue	\	Cerium Catalyst
iv	$[NEt_4]_3[Ce^{III}Cl_6]$ (**2**)	Tuna Blue	0.2 M $HOCH_3$	Alcohol, Light source
v	$[NEt_4]_3[Ce^{III}Cl_6]$ (**2**)	Tuna Blue	0.2 M $HOCH_2CCl_3$	Alcohol
vi	$[NEt_4]_3[Ce^{III}Cl_6]$ (**2**)	Tuna Blue	0.2 M ^{t}BuOH	Alcohol
vii	$[NEt_4]_3[Ce^{III}Cl_6]$ (**2**)	390 nm	0.2 M $HOCH_3$	Light source
viii	$[NEt_4]_3[Ce^{III}Cl_6]$ (**2**)	467 nm	0.2 M $HOCH_3$	Light source

Figure 2. A) Cyclohexane amination reaction conditions used for time-dependent reaction monitoring shown in plots B–D. Time progression experiments to determine the yield over time, based on B) reactions with different cerium speciation in the absence of alcohols, C) impact of alcohol additives on

reactions with $[NEt_4]_3[Ce^{III}Cl_6]$, D) use of different light sources, where Tuna Blue is a broad-spectrum light with $[NEt_4]_3[Ce^{III}Cl_6]$.

2.3 Identification of the Ce(III/IV) Species and Side Product Formation.

The control experiments described above provide important insights into the nature of the induction reaction, during which reaction of cerium(III) complexes, alcohol additives, and DBAD culminates in the generation of the cerium(IV) active photoredox catalyst, product **4b** and hydrazine side product, **4c**. To gain further insight into the mechanistic pathways for the catalytic alkane amination, we sought to address the following questions: 1) How is $HOCH_3$ involved in the cerium(III) speciation? 2) Which excited state species generates the active cerium(IV) photocatalyst from the cerium(III) pre-catalyst under blue light irradiation, cerium(III)* or DBAD*? 3) What is the active cerium(IV) catalyst for the C–H amination reaction? 4) What side reactions are observed and how do they influence the reaction mechanism?

Following our previous report and the discussion above,[30] we observed by static UV-vis absorption experiments that not only $HOCH_2CCl_3$ but also $HOCH_3$ had negligible influence on the structure or reactivity of the cerium(IV) complex $[NEt_4]_2[Ce^{IV}Cl_6]$ (**1**). Neither alcohol led to formation of cerium(IV) alkoxide species, as indicated by the lack of a blue-shifted absorption band characteristic of $[NEt_4]_2[Ce^{IV}Cl_5(OR)]$, -OR = $-OCH_3$, $-OCH_2CCl_3$. For the current work, we examined the interaction of alcohols with the cerium(III) complex $[NEt_4]_3[Ce^{III}Cl_6]$ (**2**), in which the cerium(III) cation affords labile coordination sites. For **2**, we observed no significant change in the UV-vis spectrum upon addition of $HOCH_2CCl_3$ (See Supporting Information, Section V.I). In contrast, addition of the more Lewis basic and compact $HOCH_3$ to $[NEt_4]_3[Ce^{III}Cl_6]$ (**2**) resulted in a modest difference, with a blue

shift from 332 nm to 328 nm (**Figure 3A**). This electronic transition corresponds to a cerium(III) 4f–5d transition; the small blue shift in the 4f-5d band may indicate a change in cerium(III) speciation. In order to better understand the cerium(III) speciation in the presence of $HOCH_3$, crystallization experiments were performed in which $HOCH_3$ was mixed with cerium(III) chlorides (**2** and **3**) in CH_3CN.

A variety of species were obtained upon crystallization by Et_2O diffusion into solutions of **2** or **3**. Single crystal XRD revealed the structures as: $[NEt_4]_3[Ce^{III}_2(\mu_2\text{-}Cl)_3Cl_6]$ (**3**), $[NEt_4]_2[Ce^{III}Cl_5(HOCH_3)]$ (**5**), and $[NEt_4]_3[Ce^{III}Cl_6]$ (**2**). Each structure was verified using at least five crystals, which showed identical unit cells, suggesting that each is a major component of the crystals grown under the corresponding set of conditions. It is worth noting that each crystal structure represents one of the species present in solution, and indeed, multiple cerium(III) species are presumed to coexist. Other off-cycle cerium(III) chloride methanol species that were identified from this mixture through crystallization, *e.g.* coordination polymers, are discussed in the Supporting Information, Section IV.I. The composition of these species is controlled by the amount of chloride anions and $HOCH_3$ additives, as observed in crystallization experiments. The new cerium(III) complex $[NEt_4]_2[Ce^{III}Cl_5(HOCH_3)]$ (**5**) is hypothesized to be one of the catalytically relevant cerium(III) species. Indeed, **5** comprises a significant fraction of the crystalline material obtained from mixing $HOCH_3$ (0.2 M to 5.0 M) with complex **2** in CH_3CN. Addition of chloride anion and $HOCH_3$ contribute to the formation of complex **5** (**Figure S IV.I.1**), while improving the alkane amination reaction rate (**Table S VIII.III.1**), consistent with the complex **5** as a reaction intermediate. The generation of complex $[NEt_4]_2[Ce^{IV}Cl_5(OCH_3)]$ (**6**) during the photocatalytic reaction is also consistent with the formation of complex **5**. Furthermore, we tentatively attribute the origin of the blue-shift of the UV-Vis spectra upon mixing $HOCH_3$ and **2** to

the emergence of an equilibrium that includes **5** (**Figure 3B**). No visible light absorption was observed for the mixture. It is reasonable to conclude that an excited state of **5** is probably not attained under visible light irradiation.[56]

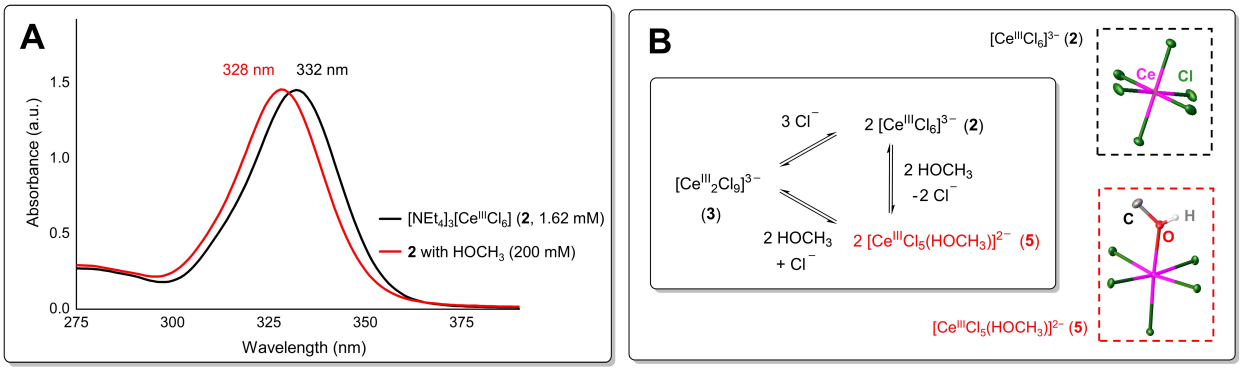

Figure 3. A) Static UV-Vis spectrum of $[NEt_4]_3[Ce^{III}Cl_6]$ (**2**, 1.62 mM) in acetonitrile (black trace) and with addition of $HOCH_3$ (0.2 M, red trace). Crystal structures for relevant cerium(III) species obtained upon Et_2O diffusion into acetonitrile solutions. B) Cerium(III) speciation of **2**, **3** and **5** in equilibrium.

To investigate the photophysics of the **2** + $HOCH_3$ system and understand how $HOCH_3$ is involved in the cerium speciation, we employed luminescence spectroscopy on a mixture of **2** with varying amounts of $HOCH_3$ in CH_3CN. The mixture was excited at 390±5 nm, and no deviation from the baseline emission spectra of **2** was observed, even with increasing concentrations of $HOCH_3$ (see Supporting Information, Section V.II). This result indicates that none of the cerium(III) species in solution could be excited under blue light irradiation above 390 nm in the presence of $HOCH_3$. Excitation at 330±5 nm resulted in the characteristic signal from the cerium(III)-chloride monomer $[NEt_4]_3[Ce^{III}Cl_6]$ (**2**) and dimer $[NEt_4]_3[Ce_2{}^{III}Cl_9]$ (**3**)**,** but no new signals were observed. This lack of luminescence intensity for **5** is likely due to a short-lived excited state compared with **2** or **3**. Notably, the equilibrium position between the cerium(III) monomer **2** and dimer **3** was perturbed by the

addition of either $HOCH_2CCl_3$ or $HOCH_3$, as judged by their relative emission band profiles (see Supporting Information, Section V). Based on the X-ray structural and spectroscopic results, the mixture of **2** + $HOCH_3$ evidently creates an equilibrium between **2**, **3**, and **5**, whose speciation is altered by the relative concentrations of Cl^- and $HOCH_3$ (**Figure 3B**).

The addition of alcohol to $[NEt_4]_3[Ce^{III}Cl_6]$ (**2**) was observed to accelerate the induction and amination reactions. Control experiments were performed, therefore, to investigate if cerium(III) and $HOCH_3$ were both necessary for DBAD to undergo a reduction reaction to hydrazine **4c**. When a mixture of DBAD with $HOCH_3$ in CH_3CN was irradiated with 467 nm light, no reaction was observed (**Figure 4A**). Similarly, combination of DBAD, $[NEt_4]_3[Ce^{III}Cl_6]$ (**2**) and cyclohexane, but without alcohol, under 467 nm irradiation formed no product after 12 h (**Table 1, entry iii**). However, upon addition of $HOCH_3$, the cyclohexane amination reaction progressed much faster, with 35% yield after 8 h (**Figure 2D, entry vii**). This result demonstrates the importance of all the components of the reaction. Based on these experiments, we postulated that DBAD reacted with $[NEt_4]_2[Ce^{III}Cl_5(HOCH_3)]$ (**5**) during the induction reaction under light irradiation to afford a catalytic cerium(IV) species. However, the possibility for a stepwise electron and proton transfer process between DBAD, Ce(III) complex **2** and $HOCH_3$ was not excluded (see Supporting Information, Section III.II). Given the isolation of complex **5** under several crystallization conditions, and the diminished reactivity of complex **2** in the absence of methanol, we favor a pathway involving reaction of **5** and DBAD under light irradiation to afford the active cerium(IV) species.

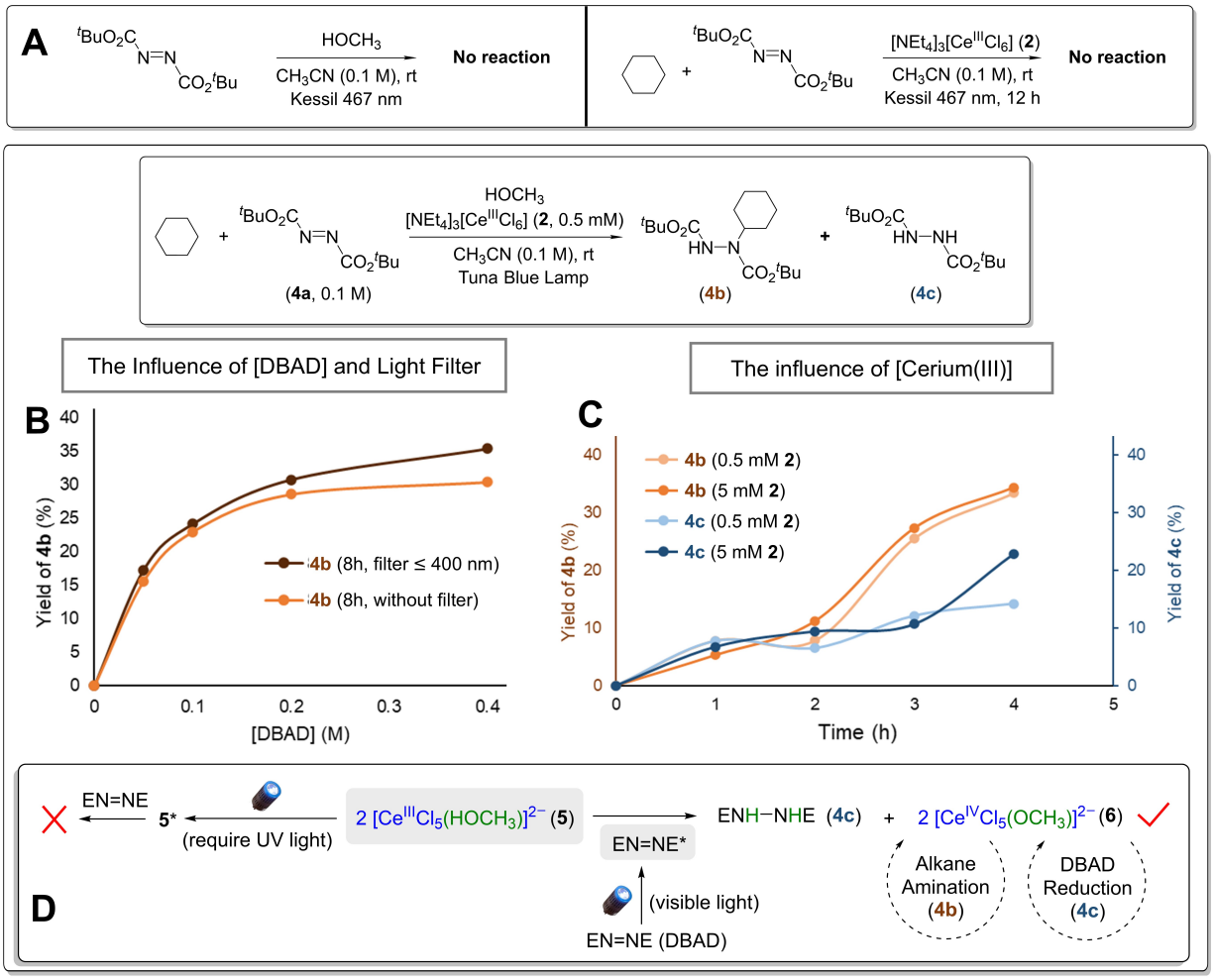

Figure 4. A) Control experiments for DBAD reaction with either $HOCH_3$ but no Ce, with catalytic **2** without methanol, or with $HOCH_3$ and catalyst **2**. B) Light filter experiment with 400 nm filter, and [DBAD] concentration dependent experiment, indicating DBAD as a photoinitiator. C) The production of **4b** and **4c** with **2** with time progression, showing no concentration dependence for **2**. D) Schematic illustration for the generation of **2** equiv of complex **6** from 1 equiv of DBAD, and the important role of the DBAD* excited state.

Two possible scenarios were envisioned for the reaction between **5** and DBAD under light irradiation: 1) the excited state of **5** reacts with ground state DBAD or 2) the excited state DBAD* reacts

with ground state **5**. We next decided to examine the possibility of the excited state of compound **5** being involved in the initiation reaction. It is noteworthy that cerium(III) species (**2**, **3**, and **5**) do not absorb in the visible light spectrum. The Tuna Blue Kessil lamp, however, emits a relatively small flux of UV light below 400 nm, which could potentially excite Ce(III) species and initiate formation of Ce(IV).[61] To eliminate the possibility of Ce(III) excitation, we used a 400 nm longpass filter on the Tuna Blue Kessil lamp to filter the higher energy UV light. A series of experiments were carried out with 0.3 M cyclohexane, 0.05–0.4 M DBAD, 0.2 M $HOCH_3$, and 5 mM complex **2** in CH_3CN, monitored at time points of 4 and 8 h. We noted negligible differences in yields with and without the filter with varying irradiation times and DBAD concentrations (**Figure 4B**). For instance, with 0.2 M DBAD, the amination conversion of **4b** progressed to 20% at 4 h and 31% at 8 h with the filter, compared to 21% at 4 h and 29% at 8 h without the filter (see Supporting Information, Section VI.I). Taken together, the data in **Figure 4B** suggests that adding a 400 nm filter to the Tuna Blue light had only minimal impact on the reaction rate, and that UV light was not necessary for the reaction to proceed. Therefore, we infer that the excited DBAD* likely serves as the visible light absorber and plays a pivotal role as the photoinitiator during the induction phase.

Building upon the hypothesis that the excited state DBAD* acts as the photoinitiator by interacting with the cerium(III) complex $[NEt_4]_2[CeCl_5(HOCH_3)]$ (**5**), we further examined the effect of cerium(III) and DBAD concentrations on the reaction. Control experiments with 0.3 M cyclohexane, 0.05–0.4 M DBAD, 0.2 M $HOCH_3$, 0.5–5 mM $[NEt_4]_3[Ce^{III}Cl_6]$ (**2**) in CH_3CN were carried out under irradiation with a Tuna Blue Kessil lamp. Analysis of the data showed a clear positive correlation between the reaction rate and DBAD concentration (**Figure 4B** and Supporting Information, Section VI.II); and a reaction rate independent of the concentrations of cerium(III) catalyst **2** (0.5 mM to 5 mM), monitored at time points of 1–4 h (**Figure 4C**). These findings highlight the essential role of DBAD light absorption, suggesting that a DBAD* excited state is crucial for converting cerium(III) to cerium(IV), independent of cerium(III) concentration.

Overall, we propose a mechanism where cerium(III) precatalyst **2** reacts with $HOCH_3$ to form complex $[NEt_4]_2[CeCl_5(HOCH_3)]$ (**5**) (**Figure 4D**). Here, 2 equiv cerium(III) complex **5** react with 1 equiv excited state DBAD* to yield 1 equiv hydrazine product **4c** and 2 equiv cerium(IV) complex **6**. Complex **6** can follow two pathways outlined in **Figure 4D**: 1) the alkane amination cycle and 2) the hydrazine reduction cycle (detailed in **Scheme 2**, *vide infra*). Next is discussed the formation of **6** and how it can be reduced to Ce(III) through a path that does not involve alkane amination.

As noted above, conversion of 0.5 mol% loading of cerium(III) precatalyst to cerium(IV) active catalyst requires the conversion of 0.25 mol% DBAD to hydrazine (**4c**). The higher-than-expected yields of the hydrazine side-product **4c** using both alcohols (Figure **3C**, Supporting Information Section VII.I) suggested that a catalytic DBAD reduction cycle is operative. We hypothesize that during the reduction of DBAD, there are direct electron and proton transfers from $HOCH_3$ to DBAD, resulting in hydrazine **4c** and primary methanol oxidation product, formaldehyde, and secondary oxidation products formed from reactive formaldehyde (**Figure 5A**, discussed below). Given that the reaction does not proceed without cerium, the process is likely mediated by the methanol adduct $[NEt_4]_2[Ce^{III}Cl_5(HOCH_3)]$ (**5**). We hypothesized that the electron transfer is driven by excited state DBAD*, oxidizing compound **5**, while the proton transfer is controlled by the reduced DBAD radical anion, [EN–NE]•$^-$, deprotonating **5**. As a result, **5** is converted to a Ce^{IV}–OCH_3 species (**6**) and the newly generated radical anion, [EN–NE]•$^-$, is protonated to give the radical ENH–EN• (**4e**). Evidence for the formation of $[NEt_4]_2[Ce^{IV}Cl_5(OCH_3)]$ (**6**) in the latter step is provided by ^{1}H-NMR spectroscopic studies on the reaction between the independently prepared deprotonated hydrazine salt, Na[EN–NHE] (**4d**), $[NEt_4]_2[Ce^{IV}Cl_6]$ (**1**), and $HOCH_3$. Upon combination of stoichiometric amounts of these species, the hydrazine product (**4c**) and $[NEt_4]_2[Ce^{IV}Cl_5(OCH_3)]$ (**6**) were observed by ^{1}H-NMR spectroscopy (23% conversion to **6**, see Supporting Information, Section X) with formation of a white solid, presumably NaCl. Returning to the catalytic cycle, once the radical [•NE–HNE] (**4e**) is generated, it could react with another molecule of complex **5** via a net-HAT from the hydroxy group to afford complex **6** as part of the induction reaction, or radical **4e** could react with complex **6** to afford

hydrazine **4c**, Ce(III) and formaldehyde, the primary oxidation product (**Scheme 2B**, *vide infra*). The DBAD reduction cycle will be further discussed in Section 2.5.

To help elucidate the methanol oxidation products formed during the reduction of DBAD to hydrazine **4c**, we carried out the reaction between cyclohexane, DBAD, $[NEt_4]_3[Ce^{III}Cl_6]$ (**2**), and $HO^{\mathbf{13}}\mathbf{C}H_3$ under the standard reaction conditions. Analyzing an aliquot from this reaction by $^{13}C\{^1H\}$ NMR spectroscopy, resonances attributed to the labelled carbon atoms were identified at 162.7, 90.8, 74.0, 54.8 and 51.2 ppm (**Figure 5B**). The peaks are attributed to secondary oxidation products formed from formaldehyde ($^{\mathbf{13}}\mathbf{C}H_2{=}O$), including $^{\mathbf{13}}\mathbf{C}H_3O^{\mathbf{13}}\mathbf{C}H_2OH$ (**7a**), the 1:1 adduct between formaldehyde and methanol at 90.8 ppm and 54.8 ppm, methyl formate, $H^{\mathbf{13}}\mathbf{C}O_2{}^{\mathbf{13}}\mathbf{C}H_3$ (**7b**), at 162.7 ppm and 51.2 ppm, and the hemi-aminal ^{t}BuO$_2$CNH-N($^{\mathbf{13}}\mathbf{C}$H$_2$OH)CO$_2{}^t$Bu (**7c**), the 1:1 reaction product between formaldehyde and hydrazine at 74.0 ppm. Other than methyl formate, these compounds are not stable towards isolation and purification. Thus, we set out to generate them independently. In the event, treatment of a formaldehyde/methanol solution with base and hydrazine **4c** led to peaks in the $^{13}C\{^1H\}$ NMR spectrum that aligned with those of CH_3OCH_2OH (**7a**) and ^{t}BuO$_2$CNH-N(CH$_2$OH)CO$_2{}^t$Bu (**7c**) from the experiments with $HO^{13}CH_3$ (see the Supporting Information, Section VII for details).

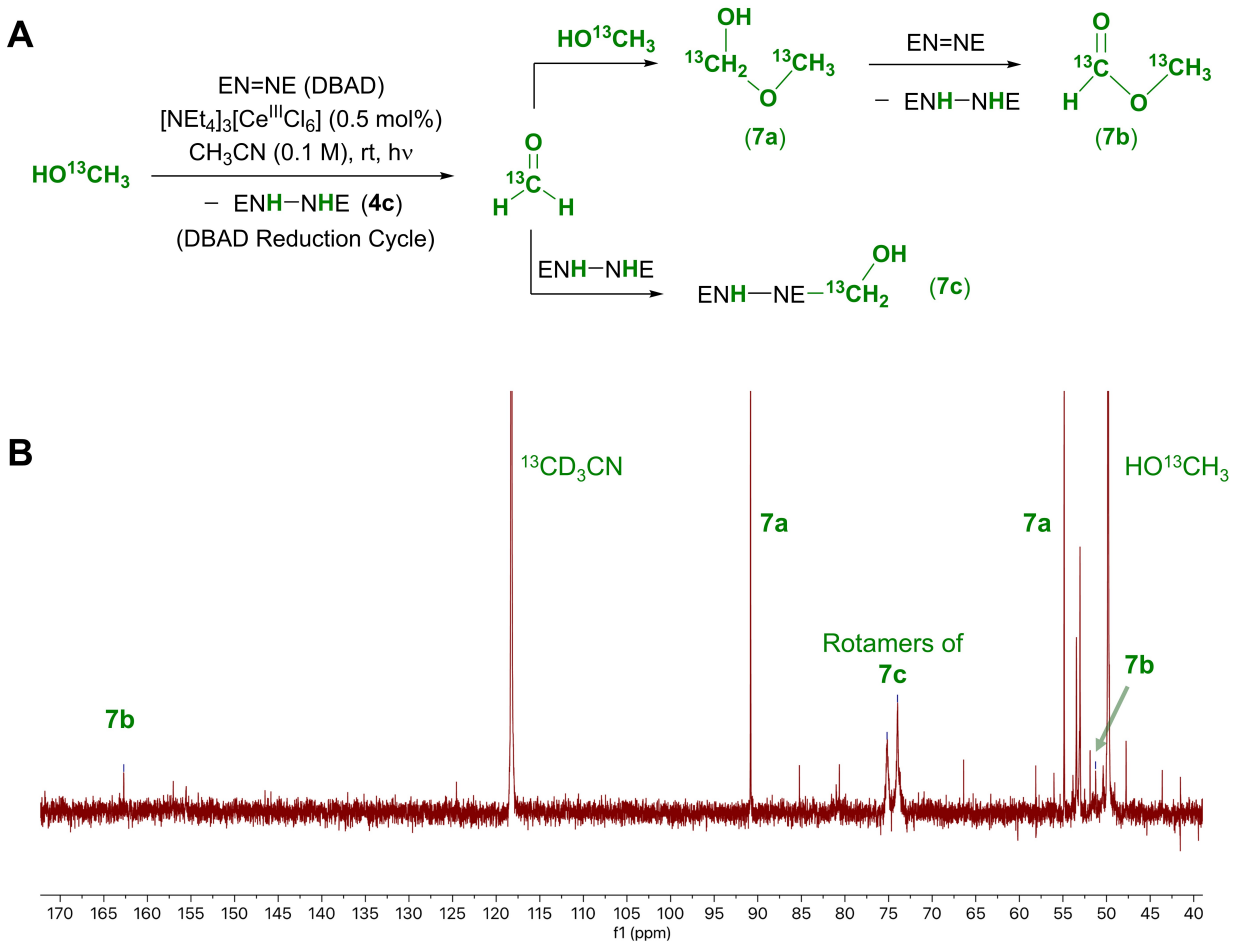

Figure 5. Reaction pathways and products analysis. A) Generation of primary oxidation product formaldehyde and secondary oxidation products **7a–c** with catalytic **2** in the presence of $HO^{13}CH_3$. B) $^{13}C\{^1H\}$ NMR of products using $HO^{13}CH_3$

2.4 Catalytic C–H Functionalization Cycles and DBAD Reduction Cycle

The next few paragraphs discuss the DBAD reduction cycle and proposed conditions-dependent C–H functionalization mechanisms. As noted earlier, we proposed that compound **6** reacts with the hydrazine radical intermediate [•NE–NEH] (**4e**) via a net-HAT from the Ce^{IV}–OCH_3 C–H to afford the hydrazine side-product NHE–NHE (**4c**), formaldehyde, and complex **2** after binding chloride. Compound

$[NEt_4]_2[Ce^{IV}Cl_5(OCH_3)]$ (**6**) is an important intermediate with competing reaction manifolds: (1) C–H activation of alkanes for **4b** generation in the alkane amination cycle, and (2) the reaction between **6** and [•NE–NEH] (**4e**) for **4c** generation in the DBAD reduction cycle (**Figure 6)**. These two pathways dominate the generation of the product **4b** and by-product **4c** and determined the **4c**/**4b** ratio. It is noteworthy that a similar reaction of **6** with [•NE–NER] (**4f**) will consume active catalyst **6** and lead to the formation of amination product **4b** (discussed in the Supporting Information Section VI.IX). Other pathways involving reaction between DBAD* and $[NEt_4]_2[Ce^{IV}Cl_5(OCH_3)]$ (**6**) or DBAD and $[NEt_4]_2[Ce^{IV}Cl_5(OCH_3)]$*, resulting in the formation of hydrazine product [NHE–NHE] **4c**, were probed. Thus, a series of experiments was carried out with 0.1–0.4 M DBAD, 0.3 M cyclohexane, 0.2 M $HOCH_3$, 5 mM complex **2** in CH_3CN and monitored at 4 and 8 h. No change in the ratio of hydrazine **4c** to C–H amination product **4b** was observed with increasing concentration of DBAD (**Figure 6A**, also see the Supplementary Information, Section VI.II). This result indicates no reaction between $[NEt_4]_2[Ce^{IV}Cl_5(OCH_3)]$ (**6**) and DBAD under light irradiation. Instead, these results better align with the cyclohexane amination and DBAD reduction pathways, where **6** either reacts with **4e** for **4c** generation or produces methoxy radical for alkane activation and **4b** formation.

Based on the above mechanistic proposal, the amount of side-product **4c** produced should be reduced by decreasing the reaction between **5** and DBAD*. Starting with Ce(IV) catalyst **6** will reduce the occurrence of the induction reaction, where **5** is converted to **6**, and diminish the generation of intermediate **4e** and eventually **4c**. Here, we have compared two different catalysts: cerium(III) complex **2** vs. cerium(IV) catalyst **6**. For these comparisons, DBAD (230 mg, 1 mmol), cyclohexane (330 μL, 3 mmol) and $HOCH_3$ (80 μL, 2 mmol) were used with 20 mol% catalyst loading. In this comparison, the hydrazine (**4c**)/product (**4b**) ratio changed from 0.016 with $[NEt_4]_2[Ce^{IV}Cl_5(OCH_3)]$ (**6**), to 0.21 with $[NEt_4]_3[Ce^{III}Cl_6]$ (**2**), (**Figure 6B**, and Supporting Information, Section VI.III). The smaller **4c/4b** ratios using cerium(IV) indicate that side-product **4c** forms less with cerium(IV) complex **6** than with the

cerium(III) complex $[NEt_4]_3[Ce^{III}Cl_6]$ (**2**). A smaller **4c**/**4b** ratio using cerium(IV) is consistent with our hypothesis.

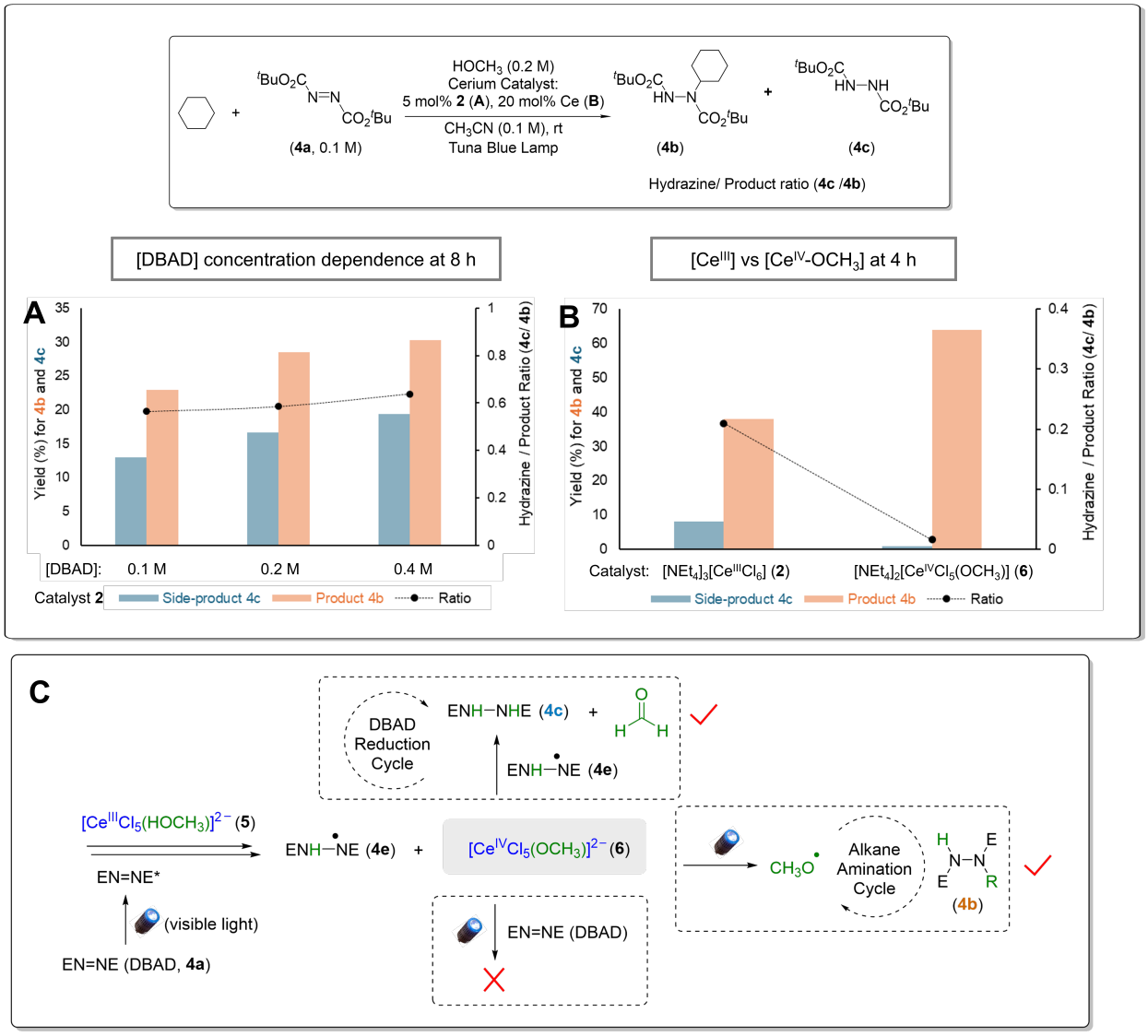

Figure 6. Cyclohexane amination reactions with cerium catalysts and $HOCH_3$ additive. A) [DBAD] concentration dependence at 8 h for the **4b**/**4c** ratio. B) Catalysts **2** and **6** at 4 h for the **4b**/**4c** ratio, with catalyst **6** (prepared by *in situ* reaction between **1** and **4d** in the presence of methanol). C) Schematic diagram outlining possible reaction pathways of intermediate **6**.

Based on the studies described above, we propose the following reaction pathways for the amination of cyclohexane initiated with $[NEt_4]_3[Ce^{III}Cl_6]$ (**2**) and $HOCH_3$, and parallel DBAD reduction (**Schemes 2A** and **2B**). In both catalytic cycles, ligand exchange between $HOCH_3$ and **2** generates $[NEt_4]_2[Ce^{III}Cl_5(HOCH_3)]$ (**5**) and releases chloride. Excited state DBAD* (EN=NE*) reacts with **5** to abstract H• (or H^+ and e^-) to afford the hydrazine radical (**4e**, •NE–NHE) and complex **6** $[NEt_4]_2[Ce^{IV}Cl_5(OCH_3)]$. Following this initial reaction, pathways within **Scheme 2B** can be envisioned for consumption of the hydrazine radical (**4e)** and generation of hydrazine (**4c**, NHE–NHE). As shown in **Scheme 2B**, following the induction pathway (bottom left box with dashed lines), radical **4e** reacts with another molecule of $[NEt_4]_2[Ce^{III}Cl_5(HOCH_3)]$ (**5**) to afford a second equivalent of **6**, thereby completing the induction reaction by conversion of Ce(III) to Ce(IV). In the second pathway along the catalytic cycle in **Scheme 2B**, hydrazine radical **4e** (in circled with red dashes) undergoes net-HAT with $[NEt_4]_2[Ce^{IV}Cl_5(OCH_3)]$ (**6**) to afford formaldehyde, hydrazine **4c**, and a cerium(III) species that can bind chloride to regenerate $[NEt_4]_3[Ce^{III}Cl_6]$ (**2**) or methanol to regenerate $[NEt_4]_2[Ce^{III}Cl_5(HOCH_3)]$ (**5**). Overall, the net reaction is a conversion of DBAD and methanol to hydrazine **4c** and formaldehyde, catalyzed by $[NEt_4]_2[Ce^{III}Cl_5(HOCH_3)]$ (**5**). When $[NEt_4]_2[Ce^{IV}Cl_5(OCH_3)]$ (**6**) is formed in the initiation reaction, it can enter the amination catalytic cycle in **Scheme 2A** by undergoing light induced ligand-to-metal charge transfer (LMCT). According to reported DFT studies,[62] either a direct generation of an alkoxy radical,[57] or through an initial generation of chlorine radical (Cl•) followed by a fast *in-situ* oxidation affords the alkoxy radical (**Scheme 2A**). The alkoxy radical (CH_3O•) performs a hydrogen atom abstraction on the alkane substrate (R–H) and generates the alkyl radical (R•), which is trapped by DBAD to afford a nitrogen centered radical, •NE–NRE (**4f**). This nitrogen centered radical species undergoes a net-HAT with the hydroxyl group of the methanol adduct **5** to afford the amination product (**4b**) and regenerates **6** to close the catalytic cycle in **Scheme 2A**. The two catalytic cycles depicted in **Scheme 2A** and **2B** are competing and result in the cyclohexane amination product (**4b, Scheme 2A**) and DBAD reduction product (**4c, Scheme 2B**). Using cerium(IV) catalyst **6** directly instead of **2** can suppress by-product **4c** and enhance the formation of amination product **4b**.

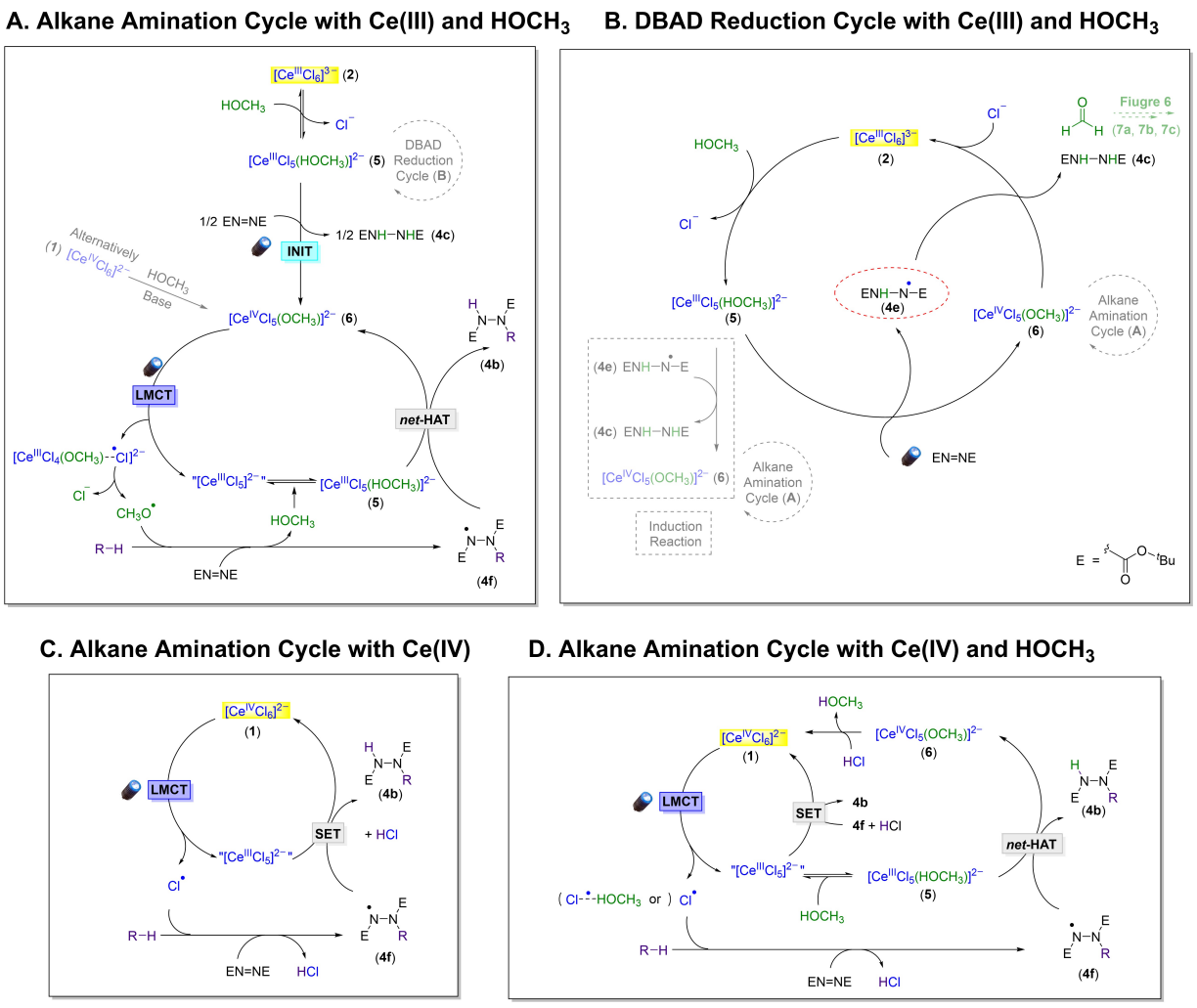

Scheme 2. A) Proposed mechanism for alkane amination using cerium(III) catalyst with $HOCH_3$. B) Induction reaction and DBAD reduction cycle using catalytic cerium(III) with $HOCH_3$. C) Previously proposed mechanism for alkane amination using $[NEt_4]_2[Ce^{IV}Cl_6]$ (**1**) catalyst without methanol. D) Elaborated mechanism for alkane amination using $[NEt_4]_2[Ce^{IV}Cl_6]$ (**1**) catalyst with $HOCH_3$.

Having mapped probable cerium(III) reaction pathways, we next sought to test our comprehensive mechanistic picture by unifying the reaction outcomes when reactions were initiated with cerium(III) or cerium(IV). The common intermediates of these two cycles are proposed to be $[NEt_4]_2[Ce^{III}Cl_5(HOCH_3)]$

(**5**) and $[NEt_4]_2[Ce^{IV}Cl_5(OCH_3)]$ (**6**). In our previous work, we proposed a cerium(IV) catalytic cycle (**Scheme 2C**) and presented mechanistic studies that indicated chlorine radical as the active HAT agent.[30] In the current study, we extend our proposed mechanism to encompass the catalytic cycle for $[NEt_4]_2[Ce^{IV}Cl_6]$ (**1**) *in the presence of HOCH₃* (**Scheme 2D**). Irradiation of **1** results in generation of chlorine radical, which reacts with R–H to generate HCl and the alkyl radical R•. The alkyl radical adds to DBAD forming the *N*-centered radical **4f** [•NE–NER]. Upon loss of Cl• from the catalyst, coordinatively unsaturated $[NEt_4]_2[Ce^{III}Cl_5]$ forms, which can bind chloride to give $[NEt_4]_3[Ce^{III}Cl_6]$ (**2**) or bind $HOCH_3$ to give $[NEt_4]_2[Ce^{III}Cl_5(HOCH_3)]$ (**5**). Complex **5** then undergoes a net-HAT from the bound methanol hydroxyl group to **4f** to afford complex **6** and product **4b**. Importantly, the HCl generated during C–H activation rapidly reacts with $[NEt_4]_2[Ce^{IV}Cl_5(OCH_3)]$ (**6**) and converts it to $[NEt_4]_2[Ce^{IV}Cl_6]$ (**1**) and methanol. The acidic conditions result in formation of $[NEt_4]_2[Ce^{IV}Cl_6]$ (**1**) at the expense of $[Ce^{IV}Cl_5(OCH_3)]^{2-}$ (**6**), thus *continuing the catalytic cycle based on C–H activation with the chlorine radical*. Additionally, the side reaction of alkane chlorination also generates HCl as discussed in a previous report,[30] contributing to the acidic nature of this reaction pathway and maintaining the active catalyst as **1** and not **6**.

Following from the proposal of these competing cycles of product formation **4b** and DBAD reduction, addition of base to $[NEt_4]_2[Ce^{IV}Cl_6]$ (**1**) and $HOCH_3$ results in the generation of $[NEt_4]_2[Ce^{IV}Cl_5(OCH_3)]$ (**6**) *in-situ* (**Scheme 2A**) to change the active catalyst from **1** to **6**. In the next section, studies on how the catalysts derived from $[NEt_4]_3[Ce^{III}Cl_6]$ and $[NEt_4]_2[Ce^{IV}Cl_6]$ exhibit different C–H selectivities, and how those selectivities provide insight into the active HAT agent are described.

2.5 Impact of Ce(III/IV) Catalysts and Alcohol Additives on C–H Bond Activation Selectivity.

In addition to understanding the influence of cerium oxidation state and alcohol additives on reactivity in the induction period, we were interested in examining their effects on selectivity in the C–H bond activation with substrates that contain inequivalent C–H bonds. In our previous studies of

photocatalysis with $[NEt_4]_2[Ce^{IV}Cl_6]$, we observed that adding alcohols provided only minor changes to the selectivity for the activation of 2,3-dimethylbutane. We proposed that $[NEt_4]_2[Ce^{IV}Cl_6]$ (**1**) generated chlorine radicals and that formation of complexes between the chlorine radicals and alcohols was responsible for the minor changes in selectivity.[30] Tertiary C–H bonds are more prone to activation with chlorine radical than primary ones due to their lower bond dissociation energies and polarity matching. For the current work, the selectivity, defined by the ratio of tertiary product (**8a**)/[tertiary (**8a**) + primary (**8b**)] C–H bond activation products, was examined in the 2,3-dimethylbutane amination reaction with DBAD under blue light irradiation. It is noteworthy that the $HOCH_3$ additive has been studied extensively by Zuo and co-workers.[28, 29, 46, 55-57, 61] We therefore focused our attention on $HOCH_3$ (40 mM–1.0 M) concentration-dependent experiments with **1** as the catalyst for the 2,3-dimethylbutane amination reaction. In the current study, we used vials for reactions at 1 mL scale and high-throughput experimentation (HTE) for reactions at a 200 μL scale and gas chromatography for quantification of the C–H functionalization selectivities. When $[NEt_4]_2[Ce^{IV}Cl_6]$ (**1**, 2.5 mM) was used to initiate catalysis, alcohols (40 mM – 1 M) altered the C–H bond activation selectivity, from 0.50 without alcohol additives, to 0.56 with 1 M $HOCH_3$ (**Figure 7A**). The change in selectivity is likely due to both radical complexation between Cl• and $HOCH_3$, and small amounts of $•OCH_3$ radical generated from complex $[NEt_4]_2[Ce^{IV}Cl_5(OCH_3)]$ (**6**). The acidic conditions, established when using **1**, favor catalyst **1** and disfavor formation of catalyst **6** (**Scheme 2D**).

To compare the effect of cerium oxidation state on selectivity, we replaced catalyst $[NEt_4]_2[Ce^{IV}Cl_6]$ (**1**) with $[NEt_4]_3[Ce^{III}Cl_6]$ (**2**) or $[NEt_4]_3[Ce_2^{III}Cl_9]$ (**3**) (**Figure 7B**). Performing the 2,3-dimethylbutane amination reaction under similar HTE conditions using $HOCH_3$ as an additive, both **2** and **3** resulted in significant increases in selectivity compared to catalyst **1**. With catalytic cerium(III) complex **2,** addition of 10 mM $HOCH_3$ resulted in a selectivity increase from 0.50 to 0.74, while 200 mM $HOCH_3$ resulted in a maximum selectivity of 0.91. When catalytic **3** was used, addition of 10 mM $HOCH_3$ increased the selectivity to 0.62, and up to 0.84 with 1 M $HOCH_3$. A small concentration of $HOCH_3$ (40 mM) was

observed to significantly change the selectivity, presumably still permitting the formation of $[NEt_4]_2[Ce^{IV}Cl_5(OCH_3)]$ (**6**). Upon increasing the equiv of $HOCH_3$ to cerium(III), there is an increase in the concentration of complex **5** at the expense of compounds **2** and **3**. Higher concentrations of **5** lead to increased amounts of cerium(IV), such as complexes **6** and **1**. The ratio of these intermediates is based on solution acidity, where basic conditions favor **6** and acidic conditions favor **1**. Overall, an increase in the formation of cerium(IV) leads to an increase of radical generation and the subsequent amination reactivity. At the same time, increasing the concentration of catalyst **6** over catalyst **1** (under basic conditions) favors methoxy radical formation, which drives the amination of 2,3-dimethylbutane with high tertiary C–H selectivity. Other additive such as NEt_4Cl also influenced the reactivity and selectivity by tuning the cerium speciation and are discussed in the Supporting Information (Section VIII.III).

These selectivity experiments were repeated on a larger scale (0.2 mmol substrate) with a Kessil Tuna Blue lamp to verify the results of the high throughput experiments. Here, reactions were carried out with 0.1 M DBAD, 0.3 M 2,3-dimethylbutane and 5 mM cerium catalyst under 24 h light irradiation, with and without $HOCH_3$ (**Figure 7C**). Without $HOCH_3$, the use of $[NEt_4]_3[Ce^{III}Cl_6]$ (**2**) gave a 5.2% yield with a selectivity of 0.50. Using $[NEt_4]_2[Ce^{IV}Cl_6]$ (**1**) gave a 60.0% yield with a selectivity of 0.46. The similar selectivity resulting from these two experiments suggests that the active HAT agents were the same in the absence of alcohol. In the presence of $HOCH_3$, however, $[NEt_4]_3[Ce^{III}Cl_6]$ (**2**) gave a 39.1% yield with a selectivity of 0.89, while $[NEt_4]_2[Ce^{IV}Cl_6]$ (**1**) gave a 61.6% yield with a selectivity of 0.43. The $HOCH_3$ additive had limited impact on catalytic $[NEt_4]_2[Ce^{IV}Cl_6]$, but the selectivity and reactivity were significantly changed when catalytic $[NEt_4]_3[Ce^{III}Cl_6]$ was used.

To evaluate the C–H selectivity over the course of the reaction with catalysts of different cerium oxidation states, time monitoring experiments (from 0.5 to 72 h, **Figure 7D, 7E**) were performed with 0.2 M $HOCH_3$. Using 5 mol% **1**, 14.8% yield of the amination product **4b** was obtained at the 0.5 h time point with a selectivity of 0.35, and 74.5% yield was obtained at 72 h with a selectivity of 0.41 (**Figure 7D**). Using 5 mol% $[NEt_4]_3[Ce^{III}Cl_6]$ (**2**), 1.6% yield was obtained after 0.5 h with a selectivity of 0.81 and 38.9%

yield was obtained after 72 h with a selectivity of 0.87 (**Figure 7E**). For each reaction, the selectivity did not change appreciably over time, indicating a systematic difference in selectivity between cerium(III) and cerium(IV) and the intermediates involved with these catalytic systems. We hypothesize that the active catalytic species starting from $[NEt_4]_2[Ce^{IV}Cl_6]$ (**1**) remains catalyst **1** and the C–H bonds are cleaved by Cl·. However, the active catalytic species starting from $[NEt_4]_3[Ce^{III}Cl_6]$ (**2**) is postulated to be $[NEt_4]_2[Ce^{IV}Cl_5(OCH_3)]$ (**6**), which generates ·OMe as the HAT mediator.

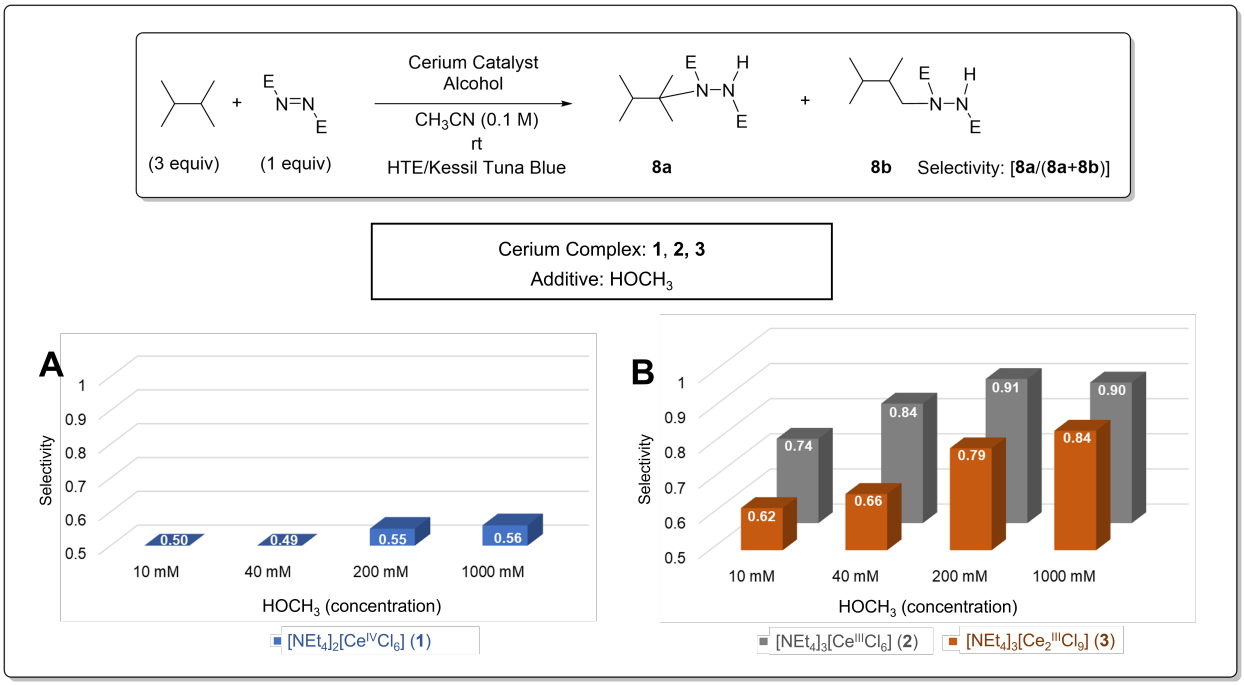

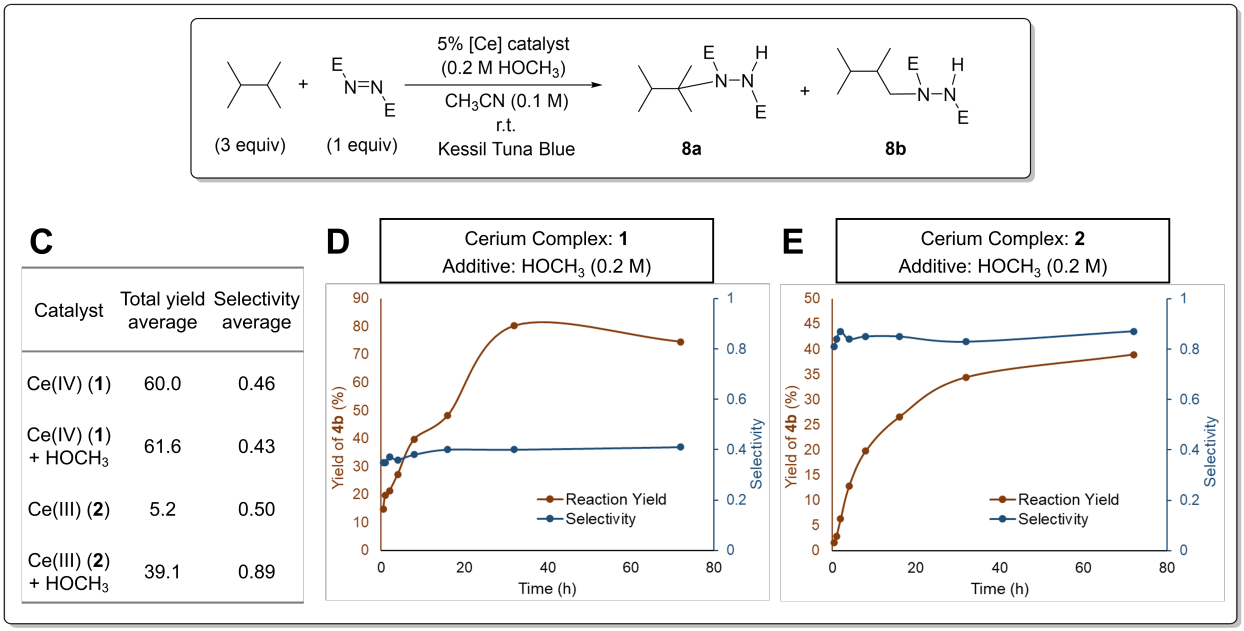

Catalyst	Total yield average	Selectivity average
Ce(IV) (**1**)	60.0	0.46
Ce(IV) (**1**) + $HOCH_3$	61.6	0.43
Ce(III) (**2**)	5.2	0.50
Ce(III) (**2**) + $HOCH_3$	39.1	0.89

Figure 7. A) Selectivity experiments using cerium(IV) catalyst **1** and alcohol additives in variable concentrations performed with high throughput experimentation. B) Selectivity experiments performed using cerium(III) catalysts (**2**, **3**) and $HOCH_3$ additive in variable concentration with high throughput experimentation. C) Confirmation of selectivity in high throughput experimentation using a conventional reaction scale with 0.2 mmol DBAD substrates in vials with Kessil Tuna blue light irradiation. D) Time progression experiment using cerium(IV) catalyst **1**. E) Time progression experiment using cerium(III) catalyst **2**.

2.6 Tuning the C–H Activation Selectivity and Unifying the Mechanistic Pictures.

An underlying pillar of our hypothesis is that the difference in the active radical species is dictated by the acidity/basicity of the reaction mixtures initiated with catalytic $[NEt_4]_2[Ce^{IV}Cl_6]$ (**1**) versus $[NEt_4]_3[Ce^{III}Cl_6]$ (**2**). The differences arise because the use of catalytic $[NEt_4]_2[Ce^{IV}Cl_6]$ (**1**) generates acid while the induction period with $[NEt_4]_3[Ce^{III}Cl_6]$ (**2**) produces base. If this hypothesis is sound, it should be possible to cross from the acidic conditions of $[NEt_4]_2[Ce^{IV}Cl_6]$, which proceeds by ·Cl-mediated catalysis, to the basic conditions of $[NEt_4]_3[Ce^{III}Cl_6]$, which is driven by $\cdot OCH_3$, by adding base or acid to the reaction mixtures. The selectivity will serve as an indicator to the active HAT agent in these experiments. Recall that stoichiometric reaction of Na[EN–NHE] (**4d**) with $[NEt_4]_2[Ce^{IV}Cl_6]$ (**1**) in the presence of $HOCH_3$ provided complex $[NEt_4]_2[Ce^{IV}Cl_5(OCH_3)]$ (**6**).

To probe this hypothesis, we set out to modulate the basicity of the amination reaction (0.1 M DBAD, 0.3 M 2,3-dimethylbutane). Under catalytic conditions with **1** (0.005 M), we obtained 80% yield with a selectivity of 0.39 (**Table 2**, **entry 9**). Conducting the same experiment with added $HOCH_3$ (0.2 M) resulted in a slight decrease in yield (63%, **entry 8**) with similar selectivity of 0.42 (monitored by GC-MS). Similar results were obtained by repeating these two experiments with monitoring by ^1H NMR (See Supporting Information, Section IX.IX). These observations are consistent with our prior report.[30] In the

presence of the base Na[NE–NHE] **4d** (0.005 M), $[NEt_4]_2[Ce^{IV}Cl_6]$ (**1**) (0.005 M) and $HOCH_3$ (0.2 M), the selectivity rose to 0.96 (**entry 1**). This high selectivity is comparable to the selectivity observed when using catalytic $[NEt_4]_3[Ce^{III}Cl_6]$ (**2**) and $HOCH_3$ (0.85 in **Table 2**, **entry 2**; 0.91 in **Figure 6B**). Crucially, this result indicates that the base additive Na[EN–NHE] **4d** changes the active HAT agent and drives a cross-over between the cycle initiated with $[NEt_4]_2[Ce^{IV}Cl_6]$ (**1**) to that observed starting from $[NEt_4]_3[Ce^{III}Cl_6]$ (**2**). These results also suggest that when $[NEt_4]_3[Ce^{III}Cl_6]$ (**2**) is used in the 2,3-dimethylbutane amination reaction in the presence of $HOCH_3$, the active catalyst is likely $[NEt_4]_2[Ce^{IV}Cl_5(OCH_3)]$ (**6**), generated under the basic conditions (**Scheme 2A**).

To further test this hypothesis, we set out to modulate the acidity of the amination reaction mixture using $[NEt_4]_3[Ce^{III}Cl_6]$ (**2**). Thus, a series of reactions with 0.3 M 2,3-dimethylbutane, 0.1 M DBAD and 0.2 M $HOCH_3$ were performed at different concentrations of HCl. As noted, using 5 mol% **2** under irradiation with a Tuna Blue Kessil lamp for 24 h, an amination reaction resulted in a yield of 35% with a selectivity of 0.85 (**entry 2**), Notably, maintaining the concentration of $HOCH_3$ (0.2 M) while adding HCl resulted in a decrease in selectivity from 0.85 (no acid) to 0.75 (0.6 mM HCl, **entry 3**), 0.72 (1.9 mM HCl, **entry 4**), 0.55 (4.4 mM HCl, **entry 5**), 0.46 (10.0 mM HCl, **entry 6**). Interestingly, addition of HCl (4.4 mM) also resulted in an increase in the amination yield (55–58% yield at 0.6–4.4 M HCl). Adding acid decreased selectivity while maintaining the reactivity, likely because the induction reaction between complex $[NEt_4]_2[Ce^{III}Cl_5(HOCH_3)]$ (**5**) and DBAD* is not affected by acidity but the reactivity is maintained (**Scheme 2D**). Under the acidic conditions, there is conversion of cerium(IV) complex $[NEt_4]_2[Ce^{IV}Cl_5(OCH_3)]$ (**6**) to $[NEt_4]_2[Ce^{IV}Cl_6]$ (**1**) in the presence of HCl, and, therefore, less side reaction to give **4c** due to diminished concentration of complex **6**. Conducting a similar experiment using 5 mol% **2**, in the absence of $HOCH_3$, resulted in a yield of 12% with a selectivity of 0.44 (**entry 7**), consistent with our hypothesis.

Overall, these experimental results indicate that the selectivity in the amination of 2,3-dimethylbutane is impacted by the presence of acid and base, and that both of these conditions are consistent with our overall mechanistic hypotheses of catalytic cycles originating from either Ce(IV) complex **1** or cerium(III) species that can be modulated through control of the acidity/basicity of the reaction medium.

Table 2. Selectivity experiments with different additives, including $HOCH_3$, HCl, Na[NE–NHE] (**4d**). The selectivity is controlled by the CH_3O• intermediate under basic conditions and Cl• intermediate under acidic conditions.

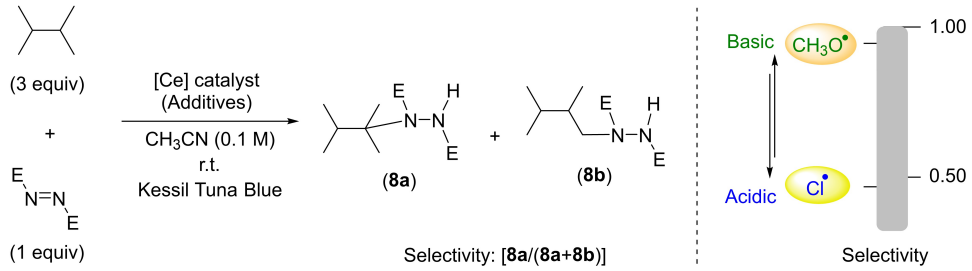

Entry	[Ce] (5 mM)	[$HOCH_3$]	[HCl] (Acid)	[**4d**] (Base)	Total yield average (%)	Selectivity average
1	$[NEt_4]_2[Ce^{IV}Cl_6]$	200 mM	\	5 mM	73	0.96
2	$[NEt_4]_3[Ce^{III}Cl_6]$	200 mM	\	\	35	0.85
3	$[NEt_4]_3[Ce^{III}Cl_6]$	200 mM	0.6 mM	\	58	0.75
4	$[NEt_4]_3[Ce^{III}Cl_6]$	200 mM	1.9 mM	\	55	0.72
5	$[NEt_4]_3[Ce^{III}Cl_6]$	200 mM	4.4 mM	\	58	0.55
6	$[NEt_4]_3[Ce^{III}Cl_6]$	200 mM	10.0 mM	\	42	0.46
7	$[NEt_4]_3[Ce^{III}Cl_6]$	\	\	\	12	0.44
8	$[NEt_4]_2[Ce^{IV}Cl_6]$	200 mM	\	\	63	0.42
9	$[NEt_4]_2[Ce^{IV}Cl_6]$	\	\	\	80	0.39

Ultimately, these studies provide a comprehensive strategy to enhance reaction yield and control selectivity through manipulation of the reaction manifolds. Major findings of this work are: 1)

The reaction rate is limited by the induction of the active cerium(IV) catalyst from the cerium(III) precursor. In the induction reaction, DBAD serves as a mild photo-oxidant to react with the cerium(III)-methanol complex. Alternatively, Ce(III) excited state provides a more effective photo-reductant to react with DBAD, but requires UV irradiation. On the other hand, Zuo has shown an effective photo-oxidant diphenylanthracene under blue light to replace the role of DBAD.[63] 2) The reaction side-product **4c** can be minimized by initiating with Ce(IV) catalysis while bypassing the induction period and reducing the DBAD reduction reaction. 3) The C–H selectivity can be tuned with acid or base additives. Adding acid directs radical formation into the Cl• manifold, while adding base steers the reactivity into the CH_3O• manifold.

3. CONCLUSIONS

Controlling C–H selectivity in the functionalization of C–H bonds is of paramount importance in the application of photoredox catalysts in modern synthetic organic chemistry. This study provides a roadmap to explore photochemical induction reactions by emphasizing how protic additives like alcohols, combined with single electron transfer from the metal center, facilitate the induction process leading to net hydrogen atom transfer (HAT) reactions. It also demonstrates how alcohols, may or may not give rise to the formation of redox-active metal alkoxides, which are precursors to alkoxy radicals. The key determinate of the nature of the radical intermediate, either M–Cl or M–OMe, and hence the identity of the active HAT agent, is the presence of acid or base *generated* during the induction phase of the catalytic reaction. Finally, the study offers insights into the crucial role of acidic and basic intermediates and their impact on the active HAT agents and the selectivity of the C–H functionalization process.

Supporting Information.

The supporting Information is available free of charge.

Additional experimental details, introduction, characterization, spectra and discussions were included in the supporting information.

Author Contributions.

All authors agree with the authorship.

AUTHOR INFORMATION

Corresponding Author

Eric J. Schelter – P. Roy and Diana T. Vagelos Laboratories, Department of Chemistry, University of Pennsylvania, 231 S. 34th St., Philadelphia, PA 19104 (USA); orcid.org/0000-0002-8143-6206; schelter@sas.upenn.edu

Patrick J. Walsh – P. Roy and Diana T. Vagelos Laboratories, Department of Chemistry, University of Pennsylvania, 231 S. 34th St., Philadelphia, PA 19104 (USA); orcid.org/0000-0001-8392-4150; pwalsh@sas.upenn.edu

Author

Qiaomu Yang – Center for Nanoscale Materials, Argonne National Laboratory, Woodridge, Illinois 60517, United States; orcid.org/0000-0002-4231-1355.

Ellen Song – P. Roy and Diana T. Vagelos Laboratories, Department of Chemistry, University of Pennsylvania, 231 S. 34th St., Philadelphia, PA 19104 (USA).

Yu Wu – P. Roy and Diana T. Vagelos Laboratories, Department of Chemistry, University of Pennsylvania, 231 S. 34th St., Philadelphia, PA 19104 (USA); orcid.org/0009-0001-6636-5008.

Chenshuai Li – P. Roy and Diana T. Vagelos Laboratories, Department of Chemistry, University of Pennsylvania, 231 S. 34th St., Philadelphia, PA 19104 (USA); orcid.org/0000-0001-7864-0778.

Michael R. Gau – P. Roy and Diana T. Vagelos Laboratories, Department of Chemistry, University of Pennsylvania, 231 S. 34th St., Philadelphia, PA 19104 (USA); orcid.org/0000-0002-4790-6980.

Jessica M. Anna – Chevron Science Center, 219 Parkman Avenue, Pittsburgh, PA 15260; orcid.org/0000-0001-5440-6987.

ACKNOWLEDGMENTS

E.J.S. thanks the U.S. Department of Energy, Office of Science, Office of Basic Energy Sciences Separations and Analysis program under Award Number DE-SC0017259 for partial support of Q.Y. P.J.W. thanks the US National Science Foundation (CHE-2154593). The project was partially supported by Vagelos Institute for Energy Science and Technology (VIEST). We also thank JASCO in the JASCO facility for Spectroscopic Excellence in the Chemistry Department at the University of Pennsylvania. E.J.S. thanks Prof. Jochen Autschbach and Dr. Xiaojuan Yu, both of the University of Buffalo, for helpful discussions. We thank Dr. Ekaterina Lapsheva for help with editing.

References

(1) Meng, X. G.; Cui, X. J.; Rajan, N. P.; Yu, L.; Deng, D. H.; Bao, X. H. Direct Methane Conversion under Mild Condition by Thermo-, Electro-, or Photocatalysis. *Chem* **2019**, *5* (9), 2296-2325. DOI: 10.1016/j.chempr.2019.05.008.
(2) Pulcinella, A.; Mazzarella, D.; Noël, T. Homogeneous catalytic C(sp^3)–H functionalization of gaseous alkanes. *Chem. Commun.* **2021**, *57* (78), 9956-9967, 10.1039/D1CC04073A. DOI: 10.1039/D1CC04073A.
(3) Gunsalus, N. J.; Koppaka, A.; Park, S. H.; Bischof, S. M.; Hashiguchi, B. G.; Periana, R. A. Homogeneous Functionalization of Methane. *Chem. Rev.* **2017**, *117* (13), 8521-8573. DOI: 10.1021/acs.chemrev.6b00739.
(4) Ravi, M.; Ranocchiari, M.; van Bokhoven, J. A. The Direct Catalytic Oxidation of Methane to Methanol—A Critical Assessment. *Angew. Chem. Int. Ed.* **2017**, *56* (52), 16464-16483, DOI: https://doi.org/10.1002/anie.201702550.
(5) Caballero, A.; Pérez, P. J. Methane as raw material in synthetic chemistry: the final frontier. *Chem. Soc. Rev.* **2013**, *42* (23), 8809-8820, DOI: 10.1039/C3CS60120J.
(6) Schwach, P.; Pan, X.; Bao, X. Direct Conversion of Methane to Value-Added Chemicals over Heterogeneous Catalysts: Challenges and Prospects. *Chem. Rev.* **2017**, *117* (13), 8497-8520. DOI: 10.1021/acs.chemrev.6b00715.

(7) Sun, L.; Wang, Y.; Guan, N.; Li, L. Methane Activation and Utilization: Current Status and Future Challenges. *Energy Technol.* **2020**, *8* (8), 1900826. DOI: https://doi.org/10.1002/ente.201900826.
(8) Tang, P.; Zhu, Q.; Wu, Z.; Ma, D. Methane activation: the past and future. *Energy & Environ. Sci.* **2014**, *7* (8), 2580-2591, DOI: 10.1039/C4EE00604F.
(9) Capaldo, L.; Ravelli, D. Hydrogen Atom Transfer (HAT): A Versatile Strategy for Substrate Activation in Photocatalyzed Organic Synthesis. *Eur. J. Org. Chem.* **2017**, *2017* (15), 2056-2071. DOI: https://doi.org/10.1002/ejoc.201601485.
(10) Li, C.; Kong, X. Y.; Tan, Z. H.; Yang, C. T.; Soo, H. S. Emergence of ligand-to-metal charge transfer in homogeneous photocatalysis and photosensitization. *Chem. Phys. Rev.* **2022**, *3* (2), 021303. DOI: 10.1063/5.0086718.
(11) Laudadio, G.; Deng, Y. C.; van der Wal, K.; Ravelli, D.; Nuno, M.; Fagnoni, M.; Guthrie, D.; Sun, Y. H.; Noel, T. C(sp(3))-H functionalizations of light hydrocarbons using decatungstate photocatalysis in flow. *Science* **2020**, *369* (6499), 92-96. DOI: 10.1126/science.abb4688.
(12) West, J. G.; Bedell, T. A.; Sorensen, E. J. The Uranyl Cation as a Visible-Light Photocatalyst for C(sp3)−H Fluorination. *Angew. Chem. Int. Ed.* **2016**, *55* (31), 8923-8927. DOI: https://doi.org/10.1002/anie.201603149.
(13) Capaldo, L.; Merli, D.; Fagnoni, M.; Ravelli, D. Visible Light Uranyl Photocatalysis: Direct C–H to C–C Bond Conversion. *ACS Catalysis* **2019**, *9* (4), 3054-3058. DOI: 10.1021/acscatal.9b00287.
(14) Hirscher, N. A.; Ohri, N.; Yang, Q.; Zhou, J.; Anna, J. M.; Schelter, E. J.; Goldberg, K. I. A Metal-Free, Photocatalytic Method for Aerobic Alkane Iodination. *J. Am. Chem. Soc.* **2021**, *143* (46), 19262-19267. DOI: 10.1021/jacs.1c08499.
(15) Kariofillis, S. K.; Doyle, A. G. Synthetic and Mechanistic Implications of Chlorine Photoelimination in Nickel/Photoredox C(sp^3)–H Cross-Coupling. *Acc. Chem. Res*. **2021**, *54* (4), 988–1000. DOI: 10.1021/acs.accounts.0c00694.
(16) Shields, B. J.; Doyle, A. G. Direct C(sp3)–H Cross Coupling Enabled by Catalytic Generation of Chlorine Radicals. *J. Am. Chem. Soc.* **2016**, *138* (39), 12719-12722. DOI: 10.1021/jacs.6b08397.
(17) Treacy, S. M.; Rovis, T. Copper Catalyzed C(sp3)–H Bond Alkylation via Photoinduced Ligand-to-Metal Charge Transfer. *J. Am. Chem. Soc.* **2021**, *143* (7), 2729-2735. DOI: 10.1021/jacs.1c00687.
(18) Wu, W.; He, X.; Fu, Z.; Liu, Y.; Wang, Y.; Gong, X.; Deng, X.; Wu, H.; Zou, Y.; Yu, N.; et al. Metal chlorides-catalyzed selective oxidation of cyclohexane by molecular oxygen under visible light irradiation. *J. Catal.* **2012**, *286*, 6-12. DOI: https://doi.org/10.1016/j.jcat.2011.09.034.
(19) Cervone, E.; Diomedi Camassei, F.; Giannini, I.; Sykora, J. Photoredox behaviour of chlorocopper(II) complexes in acetonitrile: mechanism and quantum yields. *J. Photochem.* **1979**, *11* (5), 321-332. DOI: https://doi.org/10.1016/0047-2670(79)85021-2.
(20) Kochi, J. K. Photolyses of Metal Compounds: Cupric Chloride in Organic Media. *J. Am. Chem. Soc.* **1962**, *84* (11), 2121-2127. DOI: 10.1021/ja00870a025.
(21) Lian, P.; Long, W.; Li, J.; Zheng, Y.; Wan, X. Visible-Light-Induced Vicinal Dichlorination of Alkenes through LMCT Excitation of $CuCl_2$. *Angew. Chem. Int. Ed.* **2020**, *59* (52), 23603-23608. DOI: https://doi.org/10.1002/anie.202010801.

(22) Hendrickson, D. N.; Kinnaird, M. G.; Suslick, K. S. Photochemistry of (5,10,15,20-tetraphenylporphyrinato)iron(III) halide complexes, Fe(TPP)(X). *J. Am. Chem. Soc.* **1987**, *109* (4), 1243-1244. DOI: 10.1021/ja00238a042.
(23) Kang, Y. C.; Treacy, S. M.; Rovis, T. Iron-Catalyzed Photoinduced LMCT: A 1° C–H Abstraction Enables Skeletal Rearrangements and C(sp3)–H Alkylation. *ACS Catalysis* **2021**, *11* (12), 7442-7449. DOI: 10.1021/acscatal.1c02285.
(24) Shul'pin, G. B.; Nizova, G. V.; Kozlov, Y. N. Photochemical Aerobic Oxidation of Alkanes Promoted by Iron Complexes.. *New. J. Chem.* **1996**, *20*, 1243-1256.
(25) Wu, W.; Fu, Z.; Wen, X.; Wang, Y.; Zou, S.; Meng, Y.; Liu, Y.; Kirk, S. R.; Yin, D. Light-triggered oxy-chlorination of cyclohexane by metal chlorides. *Appl. Catal. A Gen.* **2014**, *469*, 483-489. DOI: https://doi.org/10.1016/j.apcata.2013.08.045.
(26) Jin, Y.; Zhang, Q.; Wang, L.; Wang, X.; Meng, C.; Duan, C. Convenient C(sp3)–H bond functionalisation of light alkanes and other compounds by iron photocatalysis. *Green Chem.* **2021**, *23* (18), 6984-6989, 10.1039/D1GC01563J. DOI: 10.1039/D1GC01563J.
(27) Gygi, D.; Gonzalez, M. I.; Hwang, S. J.; Xia, K. T.; Qin, Y.; Johnson, E. J.; Gygi, F.; Chen, Y.-S.; Nocera, D. G. Capturing the Complete Reaction Profile of a C–H Bond Activation. *J. Am. Chem. Soc.* **2021**, *143* (16), 6060-6064. DOI: 10.1021/jacs.1c02630.
(28) An, Q.; Wang, Z.; Chen, Y.; Wang, X.; Zhang, K.; Pan, H.; Liu, W.; Zuo, Z. Cerium-Catalyzed C–H Functionalizations of Alkanes Utilizing Alcohols as Hydrogen Atom Transfer Agents. *J. Am. Chem. Soc.* **2020**, *142* (13), 6216-6226. DOI: 10.1021/jacs.0c00212.
(29) Hu, A.; Guo, J.-J.; Pan, H.; Zuo, Z. Selective functionalization of methane, ethane, and higher alkanes by cerium photocatalysis. *Science* **2018**, *361* (6403), 668-672. DOI: 10.1126/science.aat9750.
(30) Yang, Q.; Wang, Y.-H.; Qiao, Y.; Gau, M.; Carroll, P. J.; Walsh, P. J.; Schelter, E. J. Photocatalytic C–H activation and the subtle role of chlorine radical complexation in reactivity. *Science* **2021**, *372* (6544), 847-852. DOI: 10.1126/science.abd8408.
(31) Yin, H.; Jin, Y.; Hertzog, J. E.; Mullane, K. C.; Carroll, P. J.; Manor, B. C.; Anna, J. M.; Schelter, E. J. The Hexachlorocerate(III) Anion: A Potent, Benchtop Stable, and Readily Available Ultraviolet A Photosensitizer for Aryl Chlorides. *J. Am. Chem. Soc.* **2016**, *138* (50), 16266-16273. DOI: 10.1021/jacs.6b05712.
(32) Costanzo, L. L.; Pistarà, S.; Condorelli, G. Photoreduction of cerium(IV) hexachloride in acetonitrile. *J. Photochem.* **1983**, *21* (1), 45-51. DOI: https://doi.org/10.1016/0047-2670(83)80006-9.
(33) Wang, Y.-H.; Yang, Q.; Walsh, P. J.; Schelter, E. J. Light-mediated aerobic oxidation of C(sp3)–H bonds by a Ce(iv) hexachloride complex. *Org. Chem. Front.* **2022**, *9* (10), 2612-2620, 10.1039/D2QO00362G. DOI: 10.1039/D2QO00362G.
(34) Yamane, M.; Kanzaki, Y.; Mitsunuma, H.; Kanai, M. Titanium(IV) Chloride-Catalyzed Photoalkylation via C(sp^3)–H Bond Activation of Alkanes. *Org. Lett.* **2022**, *24* (7), 1486-1490. DOI: 10.1021/acs.orglett.2c00138.
(35) Panetti, G. B.; Yang, Q.; Gau, M. R.; Carroll, P. J.; Walsh, P. J.; Schelter, E. J. Discovery and mechanistic investigation of photoinduced sp3 C–H activation of hydrocarbons by the simple anion hexachlorotitanate. *Chem. Catal.* **2022**, *2* (4), 853-866. DOI: https://doi.org/10.1016/j.checat.2022.02.013.
(36) Yang, Q. M.; Wang, Y. H.; Qiao, Y. S.; Gau, M.; Carroll, P. J.; Walsh, P. J.; Schelter, E. J. Photocatalytic C-H activation and the subtle role of chlorine radical complexation in reactivity. *Science* **2021**, *372* (6544), 847-852. DOI: 10.1126/science.abd8408.

(37) Zhang, K. N.; Chang, L.; An, Q.; Wang, X.; Zuo, Z. Dehydroxymethylation of Alcohols Enabled by Cerium Photocatalysis. *J. Am. Chem. Soc.* **2019**, *141* (26), 10556-10564. DOI: 10.1021/jacs.9b05932.
(38) Hu, A. H.; Guo, J. J.; Pan, H.; Zuo, Z. W. Selective functionalization of methane, ethane, and higher alkanes by cerium photocatalysis. *Science* **2018**, *361* (6403), 668-672. DOI: 10.1126/science.aat9750.
(39) Hu, A. H.; Guo, J. J.; Pan, H.; Tang, H. M.; Gao, Z. B.; Zuo, Z. W. delta-Selective Functionalization of Alkanols Enabled by Visible-Light-Induced Ligand-to-Metal Charge Transfer. *J. Am. Chem. Soc.* **2018**, *140* (5), 1612-1616. DOI: 10.1021/jacs.7b13131.
(40) Hu, A. H.; Chen, Y. L.; Guo, J. J.; Yu, N.; An, Q.; Zuo, Z. W. Cerium-Catalyzed Formal Cycloaddition of Cycloalkanols with Alkenes through Dual Photoexcitation. *J. Am. Chem. Soc.* **2018**, *140* (42), 13580-13585. DOI: 10.1021/jacs.8b08781.
(41) Guo, J. J.; Hu, A. H.; Zuo, Z. W. Photocatalytic alkoxy radical-mediated transformations. *Tetrahedron Lett.* **2018**, *59* (22), 2103-2111. DOI: 10.1016/j.tetlet.2018.04.060.
(42) Guo, J. J.; Hu, A. H.; Chen, Y. L.; Sun, J. F.; Tang, H. M.; Zuo, Z. W. Photocatalytic C-C Bond Cleavage and Amination of Cycloalkanols by Cerium(III) Chloride Complex. *Angew. Chem. Int. Ed.* **2016**, *55* (49), 15319-15322. DOI: 10.1002/anie.201609035.
(43) Chen, Y. L.; Du, J. B.; Zuo, Z. W. Selective C-C Bond Scission of Ketones via Visible-Light-Mediated Cerium Catalysis. *Chem* **2020**, *6* (1), 266-279. DOI: 10.1016/j.chempr.2019.11.009.
(44) An, Q.; Wang, Z. Y.; Chen, Y. G.; Wang, X.; Zhang, K. N.; Pan, H.; Liu, W. M.; Zuo, Z. W. Cerium-Catalyzed C-H Functionalizations of Alkanes Utilizing Alcohols as Hydrogen Atom Transfer Agents. *J. Am. Chem. Soc.* **2020**, *142* (13), 6216-6226. DOI: 10.1021/jacs.0c00212.
(45) Chen, H., Hu, A., Chang, L., An, Q., Pan, H. and Zuo, Z. Direct Conversions of Methane via Homogeneous Processes. In *The Chemical Transformations of C1 Compounds*, Wiley-VCH, 2022.
(46) Chen, Y.; Wang, X.; He, X.; An, Q.; Zuo, Z. Photocatalytic Dehydroxymethylative Arylation by Synergistic Cerium and Nickel Catalysis. *J. Am. Chem. Soc.* **2021**, *143* (13), 4896-4902. DOI: 10.1021/jacs.1c00618.
(47) Du, J.; Yang, X.; Wang, X.; An, Q.; He, X.; Pan, H.; Zuo, Z. Photocatalytic Aerobic Oxidative Ring Expansion of Cyclic Ketones to Macrolactones by Cerium and Cyanoanthracene Catalysis. *Angew. Chem. Int. Ed.* **2021**, *60* (10), 5370-5376. DOI: https://doi.org/10.1002/anie.202012720.
(48) Mereshchenko, A. S.; Olshin, P. K.; Myasnikova, O. S.; Panov, M. S.; Kochemirovsky, V. A.; Skripkin, M. Y.; Moroz, P. N.; Zamkov, M.; Tarnovsky, A. N. Ultrafast Photochemistry of Copper(II) Monochlorocomplexes in Methanol and Acetonitrile by Broadband Deep-UV-to-Near-IR Femtosecond Transient Absorption Spectroscopy. *J. Phys. Chem. A* **2016**, *120* (11), 1833-1844. DOI: 10.1021/acs.jpca.5b12509.
(49) Mereshchenko, A. S.; Pal, S. K.; Karabaeva, K. E.; El-Khoury, P. Z.; Tarnovsky, A. N. Photochemistry of Monochloro Complexes of Copper(II) in Methanol Probed by Ultrafast Transient Absorption Spectroscopy. *J. Phys. Chem. A* **2012**, *116* (11), 2791-2799. DOI: 10.1021/jp208532u.
(50) BÜHler, R. E.; Ebert, M. Transient Charge-transfer Complexes with Chlorine Atoms by Pulse Radiolysis of Carbon Tetrachloride Solutions. *Nature* **1967**, *214* (5094), 1220-1221. DOI: 10.1038/2141220a0.

(51) Troian-Gautier, L.; Turlington, M. D.; Wehlin, S. A. M.; Maurer, A. B.; Brady, M. D.; Swords, W. B.; Meyer, G. J. Halide Photoredox Chemistry. *Chem. Rev.* **2019**, *119* (7), 4628-4683. DOI: 10.1021/acs.chemrev.8b00732.
(52) Russell, G. A. Solvent Effects in the Reactions of Free Radicals and Atoms. II. Effects of Solvents on the Position of Attack of Chlorine Atoms upon 2,3-Dimethylbutane, Isobutane and 2-Deuterio-2-methylpropane1. *J. Am. Chem. Soc.* **1958**, *80* (18), 4987-4996. DOI: 10.1021/ja01551a056.
(53) Jodkowski, J. T.; Rayez, M.-T.; Rayez, J.-C.; Bérces, T.; Dóbé, S. Theoretical Study of the Kinetics of the Hydrogen Abstraction from Methanol. 2. Reaction of Methanol with Chlorine and Bromine Atoms. *J. Phys. Chem. A* **1998**, *102* (46), 9230-9243. DOI: 10.1021/jp980846d.
(54) Rohe, S.; Morris, A. O.; McCallum, T.; Barriault, L. Hydrogen Atom Transfer Reactions via Photoredox Catalyzed Chlorine Atom Generation. *Angew. Chem. Int. Ed.* **2018**, *57* (48), 15664-15669. DOI: 10.1002/anie.201810187.
(55) Hu, A.; Guo, J.-J.; Pan, H.; Tang, H.; Gao, Z.; Zuo, Z. δ-Selective Functionalization of Alkanols Enabled by Visible-Light-Induced Ligand-to-Metal Charge Transfer. *J. Am. Chem. Soc.* **2018**, *140* (5), 1612-1616. DOI: 10.1021/jacs.7b13131.
(56) Guo, J.-J.; Hu, A.; Chen, Y.; Sun, J.; Tang, H.; Zuo, Z. Photocatalytic C−C Bond Cleavage and Amination of Cycloalkanols by Cerium(III) Chloride Complex. *Angew. Chem. Int. Ed.* **2016**, *55* (49), 15319-15322. DOI: https://doi.org/10.1002/anie.201609035.
(57) An, Q.; Xing, Y.-Y.; Pu, R.; Jia, M.; Chen, Y.; Hu, A.; Zhang, S.-Q.; Yu, N.; Du, J.; Zhang, Y.; et al. Identification of Alkoxy Radicals as Hydrogen Atom Transfer Agents in Ce-Catalyzed C–H Functionalization. *J. Am. Chem. Soc.* **2023**, *145* (1), 359-376. DOI: 10.1021/jacs.2c10126.
(58) Abou-Chahine, F.; Preston, T. J.; Dunning, G. T.; Orr-Ewing, A. J.; Greetham, G. M.; Clark, I. P.; Towrie, M.; Reid, S. A. Photoisomerization and Photoinduced Reactions in Liquid CCl4 and CHCl3. *J. Phys. Chem. A* **2013**, *117* (50), 13388-13398. DOI: 10.1021/jp406687x.
(59) Wang, G.-Z.; Liu, D.-G.; Liu, M.-T.; Fu, Y. Photocatalyst- and additive-free site-specific C(sp3)–H hydrazination of glycine derivatives and peptides. *Green Chem.* **2021**, *23* (14), 5082-5087, 10.1039/D1GC01210J. DOI: 10.1039/D1GC01210J.
(60) Zhou, C.; Huang, X.; Hu, Y.; Wu, J.; Zheng, Y.; Zhang, X. Catalyst-free visible light-induced decarboxylative amination of glycine derivatives with azo compounds. *New J. Chem.* **2022**, *46* (2), 465-469, 10.1039/D1NJ05079F. DOI: 10.1039/D1NJ05079F.
(61) Zhang, K.; Chang, L.; An, Q.; Wang, X.; Zuo, Z. Dehydroxymethylation of Alcohols Enabled by Cerium Photocatalysis. *J. Am. Chem. Soc.* **2019**, *141* (26), 10556-10564. DOI: 10.1021/jacs.9b05932.
(62) Li, W.; Wang, J.; Fang, W.; Wu, L.; Chen, X. Co-function Mechanisms of Chlorine and Alkoxy Radicals in Cerium-Catalyzed C–H Functionalization of Alkane Mediated by Visible Light. *J. Phys. Chem. Lett.* **2023**, *14* (26), 6187-6192. DOI: 10.1021/acs.jpclett.3c01049.
(63) Hu, A.; Chen, Y.; Guo, J.-J.; Yu, N.; An, Q.; Zuo, Z. Cerium-Catalyzed Formal Cycloaddition of Cycloalkanols with Alkenes through Dual Photoexcitation. *J. Am. Chem. Soc.* **2018**, *140* (42), 13580-13585. DOI: 10.1021/jacs.8b08781.